Development of Solid-State Electrolyte for using fast lithium ion conducting inorganic material in Solid-State Lithium Metal Batteries (SSLMBs)

A write-up for thesis submitted in partial fulfilments of the requirements for award of the degree of

Master of Technology in Nanoscience and Technology

Under the guidance of

Dr. Mir Wasim Raja, Senior Scientist

(Energy Materials and Devices Division, CSIR-CGCRI)

By

TANDRIMA SAHA

Registration number: 163822 of 2022-23
Class Roll No.: 002230701023
Examination Roll No: M4NST24020
ACADEMIC YEAR: 2023-2024

DEPARTMENT: SCHOOL OF MATERIALS SCIENCE AND NANOTECHNOLOGY

Jadavpur University

Duration: 01.09.2023-31.05.2024

Energy Materials & Devices Division, CSIR-CGCRI (Kolkata)

School of Materials Science and Nano Technology
Jadavpur University, Kolkata- 700032, INDIA.

CERTIFICATE OF RECOMMENDATION

We hereby recommend that the thesis entitled as "Development of Solid-State Electrolyte for using fast lithium ion conducting inorganic material in Solid-State Lithium Metal Batteries (SSLMBs)", prepared by Ms. Tandrima Saha (Class Roll No 002230701023, Registration No. 163822 of 2022-23, Examination Roll No. M4NST24020 under our guidance, be accepted in partial fulfilment of the requirement for the award of the Degree of Master of Technology in Nano Science and Technology from the School of Materials Science and Nano Technology of Jadavpur University.

_____ _____

Director
Dr. Mohua Ghosh Chowdhuri (Director),
School of Materials Science & Nanotechnology
Jadavpur University

Thesis Supervisor
Dr. Mir Wasim Raja (Senior Scientist),
Energy Materials & Devices Division
CSIR-CGCRI, Kolkata

_____ _____

Thesis Advisor
Dr. Chandan Kumar Ghosh (Assistant Professor),
School of Materials Science and Nanotechnology
Jadavpur University

Dean-FISLM,
Jadavpur University,
Kolkata – 700 032

School of Materials Science and Nano Technology

Jadavpur University, Kolkata- 700032, INDIA

CERTIFICATE OF APPROVAL

The foregoing thesis titled “Development of Solid-State Electrolyte for using fast lithium ion conducting inorganic material in Solid-State Lithium Metal Batteries (SSLMBs)" was hereby approved by the committee of the final examination for evaluation of the thesis as a credited study of an engineering subject carried out and presented by Ms. Tandrima Saha (Class Roll No: 002230701023, Registration No. 163822 of 2022-23, Examination Roll No. M4NST24020) in a manner satisfactory to warrant its acceptance as a prerequisite to the degree of Master of Technology in Nano Science and Technology. It was understood by this approval, the undersigned do not necessarily endorse or approve any statement made, opinion expressed or conclusion drawn therein but approve the thesis only for the purpose for which it was submitted. Committee of final examination for evaluation of thesis.

_____ _____

_____ _____

_____ _____

_____ _____

Signature **Date**

School of Materials Science and Nano Technology
Jadavpur University, Kolkata- 700032, INDIA.

Declaration of Originality and Compliance of Academic Ethics

I hereby declare that this thesis titled " *Development of Solid-State Electrolyte for using fast lithium ion conducting inorganic material in Solid-State Lithium Metal Batteries (SSLMBs*)" contains literature survey and original research work by the undersigned candidate, as part of my Degree of Master of Technology in Nanoscience and Technology. All Information in this document has been obtained and presented in accordance with academic rules and ethical conduct.

I also declare that, as required by these rules and conduct, I have fully cited and referenced all material results that were not original to this work.

Name (Block Letters): TANDRIMA SAHA

Class Roll No: 002230701023

Registration No: 163822 of 2022-23

Examination Roll No: M4NST24020

_____

Signature with date

ACKNOWLEDGEMENT

I extend my heartfelt gratitude to everyone who helped elevate these ideas from basic concepts to something substantial. I am deeply thankful to my thesis supervisor, Dr. Mir Wasim Raja, for his strong support, patience, and constant availability for technical discussions. Special thanks to my advisor, Professor Dr. Chandan Kumar Ghosh, for his continuous support, guidance, and encouragement during my thesis work. I am also grateful to Ph.D. scholars Kuntal Ghosh and Mononita Das, whose valuable suggestions, support, and knowledge guided me throughout my research. I would like to thank all the members of the EMDD division at CSIR-CGCRI, Kolkata, and the School of Materials Science & Nanotechnology at Jadavpur University, Kolkata, for providing me the opportunity to carry out my M.Tech thesis work in a resourceful and supportive research environment. My appreciation also goes to my fellow lab mates at the Energy Materials & Devices Division, CSIR-CGCRI Kolkata, and the Faculty of Engineering and Technology, Jadavpur University, Kolkata, for their moral support throughout my thesis work. Above all, my deepest appreciation goes to my parents for their unwavering faith, unconditional love, support, encouragement, and quiet patience.

Tandrima Saha

School of Materials Science & Nanotechnology,

Jadavpur University,

Kolkata

INDEX

Chapter No.	Subject	Pages
	Abstract	**12**
	Introduction	**13-14**
1.		**16**
	Prospect of Solid-State Lithium Metal Batteries (SSLMBs)	**17-24**
	1.1 Electrolytes in Lithium Batteries- Liquid, Polymer & Solid	**24-25**
	1.2 Types of solids electrolyte (SEs)	**25-29**
	1.3 Solid polymer electrolytes (SPEs)	**29-30**
	1.4 Solid Composite electrolytes (SCEs)	**30-31**
	1.5 Inorganic ceramic electrolytes (ICEs)	
2.	**Crystalline electrolytes, glass and glass-ceramic based electrolytes**	
	2.1 Crystalline electrolytes: LISICON, Thio-LISICON, Garnet, Perovskite, NASICON	**33**
	2.2 Glass based electrolytes	**34**
	2.3 Glass-ceramic based electrolytes	**34-35**
	NASICONs and $LiA_2^{IV}(PO_4)_3$ [A^{IV}: Ti, Zr, Ge, Hf]	**35-37**
	2.4 Structure of NASICON	**37**
	2.5 Physio-chemical properties	**37-38**
	2.6 Electrochemistry of NASICON in SSLMBs	
3.	**Studies on LATP; $Li_{1.5}Al_{0.5}Ti_{1.5}(PO_4)_3$**	
	3.1 Synthesis: Advanced Solid-State Synthesis	**40-41**
	3.2 Structural and Microstructural properties	**42-52**
	3.3 Thermal Analysis of the microstructure	**52-54**
	3.4 Density calculation using Archimedes principle	**55-57**
4.	**Electrochemical Cell performance $Li_{1.5}Al_{0.5}Ti_{1.5}(PO_4)_3$ in SSBs**	**59-60**
	4.1 Ionic transport properties	**61-72**
	4.2 Electrochemical cell performance studies	**72-77**
	4.3 Symmetric cell and Plating/striping behavior	**77-78**
	4.4 Post electrochemical studies	
5.	**Conclusions**	**79**
6.	**Future work**	**80**
7.	**References**	**81-83**

SI No.	List of Figures	Page
1.	The history of NASICON superionic conductor solid-state electrolyte	16
2.	Schematic of Liquid electrolyte	23
3.	Different types of solid polymer-based electrolytes and their corresponding performances. (Ref. taken from: DOI: 10.1039/D2YA00043A (Review Article) *Energy Adv.*, 2022, 1, 457-510)	25
4.	Schematic illustration of the lithium-ion transfer across (a) a crystalline polymer, (b) crystalline polymer with nanofillers, and (c) modified polymer with nanofillers	29
5.	Illustration depicting the structure of fillers and template polymers used in developing CSEs. The graphic also highlights the overarching benefits of using CSEs. [2] (Ref. taken from Nguyen, A.-G.; Park, C.-J. Insights into Tailoring Composite Solid Polymer Electrolytes for Solid-State Lithium Batteries. *J. Member. Sci.* 2023, *675*, 121552)	30
6.	Illustration of Inorganic ceramic polymer as electrolyte	31
7.	Comparisons of types of solid electrolytes (a) SPE (b) SCE (c) ICE	31
8.	Crystal structure of NASICON type solid electrolyte. Red spheres are oxygen ions; greens are lithium ions; blue spheres are titanium ions; violets are phosphorous ions. (For interpretation of the references to colour in this figure legend, the reader is referred to the web version of this article.) Reference has been taken from N. Tolganbek et al. / Materials Today: Proceedings 25 (2020) 97–100	36

9.	A) The rhombohedral structure showing A1 and A2 sites; (Ref.Springer Science+Business Media, LLC 2011); (B) the different bottlenecks of monoclinic sodium superionic conductors structure; (copyright 2016 American Chemical Society); the unit cells and Na^+ migration channels (C) rhombohedral; and (D) monoclinic $Na_3Zr_2Si_2PO_{12}$.(Ref copyright 2021 Wiley-VCH GmbH).	38
10.	Reagents used for the synthesis of LATP	41
11.	Synthesis process of LATP solid electrolyte by ball milling	42
12.	a) XRD graph plotted for pure LATP calcined at 900^{o}C (b)LATP plotted with LTP data #PDF-350754 confirming the formation of LATP powder. (c) XRD of LATP powder formed plotted along LTP(#PDF-350754) along with probable impurities that might form $AlPO_4$, TiO_2	43
13.	XRD data of pure LATP and various concentration of PEG-200 added during the 2nd calcination at 900^{o}C of the LATP initially calcined at intermediate temperature of 500^{o}C	44
14.	FESEM images for LATP calcined at 500^{o}C	46
15.	EDX of LATP calcined at 500^{o}C	46
16.	FESEM images of (a)Pure LATP (b)LATP+5%wt PEG (c) LATP+10%wt PEG (d) LATP+15%wt PEG calcined at 900^{o}C	47
17.	FESEM images of LATP and 25%wt PEG calcined at 900^{o}C	48
18.	EDX of (a)LATP+5%PEG (b) LATP+10%PEG (c) LATP+15%PEG calcined at 900^{o}C	49
19.	FTIR of (a)Pure LATP (b)LATP+10%PEG (c) LATP+15%PEG (d) LATP+25%PEG calcined at 900^{o}C	50
20.	DLS of (a)Pure LATP (b)LATP+10%PEG (c) LATP+15%PEG	51

(d) LATP+25%PEG calcined at 900^{o}C

21. Graphical comparison of average particle size for pristine and PEG variation in LATP 52

22. TG-DTA for ash synthesized LATP powder dried after ball milling for 24hours done at temperature (0-1200^{o}C). 53

23. TG-DTA for (a) LATP+10% PEG (b) LATP+15% PEG (c) LATP+25% PEG 54

24. Experimental procedure to measure the density of LATP using Archimedes method 56

25. The relation between density calculated by Archimedes principle and the green density calculated 57

26. Process of preparing LATP pellet for electrochemical studies 60

27. EIS data of pure LATP at variation of temperature from RT-120^{o}C 62

28. Activation energy plotted from (RT-120) ^{o}C for pristine LATP 63

29. EIS data of LATP-5 at variation of temperature from RT-120^{o}C 64

30. Activation energy plotted from (RT-120) ^{o}C for LATP-5 65

31. EIS data of LATP-10 at variation of temperature from RT-120^{o}C 66

32. Activation energy plotted from (RT-120) ^{o}C for LATP-10 67

33. EIS data of LATP-15 at variation of temperature from RT-120^{o}C 67

34. Activation energy plotted from (RT-120)^{o}C for LATP-15 68

35. EIS data of LATP-25 at variation of temperature from RT-100^{o}C 69

36.	Activation energy plotted from (30-100)^{o}C for LATP-25	70
37.	EIS data of pure LATP and PEG% variation at room temperature	71
38.	Ionic Conductivity VS PEG% variation plotted at room temperature(30^{o}C)	72
39.	Activation Energy VS PEG% variation	72
40.	EIS for the symmetric cell of the pristine LATP cell (Li-LATP-Li)	73
41.	Reaction between LATP and lithium foil in symmetric cell	74
42.	Electrochemical galvanostatic profile of Li/ LATP-10/Li symmetric cell	74
43.	Current vs Time graph for the Li/LATP-10/Li for 90 hour	75
44.	EIS for the symmetric cell of the LATP-10 cell (Li-LATP-10-Li)	75
45	Enlarged cycling profiles from (a) 0-10hours [1st 10 hours] (b)40-50 hours (c) 80-90hours [last 10 cycles]	76
46.	Current vs Time graph for the Li/LATP/Li for 45 hours.	77
47.	Electrochemical galvanostatic profile of Li/ LATP/Li symmetric cell	78
48.	(a) DAY 1 (b)DAY 5 (c) DAY 10--EIS taken for the symmetric cell with pristine Li-LATP-Li & Li-LATP+PEG-Li	79

SI. No.	Table	Page
1.	Brief comparison among the electrolytes	17-18
2.	Brief comparison among the type of solvents in liquid electrolyte	19
3.	Brief comparison among the type of salts in liquid electrolyte	20-21
4.	Brief comparison among the type of additives used in liquid electrolyte	21-22
5.	Properties of NASICON	37
6.	Green density calculation.	55
7.	Density calculation using Archimedes principle	56
8.	Data for Conductivity calculation at a temperature of (RT-120) ^{o}C	63
9.	Data for Activation energy calculation at a temperature of (RT-120) ^{o}C	63
10.	Data for Conductivity calculation at a temperature of (RT-120) ^{o}C	65
11.	Data for Activation energy calculation at a temperature of (RT-120) ^{o}C	65
12.	Data for Conductivity calculation at a temperature of (RT-120) ^{o}C	66
13.	Data for Activation energy calculation at a temperature of (RT-120) ^{o}C	66
14	Data for Conductivity calculation for LATP-15 at a temperature of (RT-120)^{o}C	68
15.	Data for Activation energy calculation for LATP-15 at a temperature of (RT-120)^{o}C	68
16.	Data for Conductivity calculation for LATP-25 at a temperature of (RT-120)^{o}C	69
17	Data for Activation energy calculation for LATP-25 at a temperature of (RT-100)^{o}C	69

ABSTRACT

All solid-state lithium-ion batteries (ASSLBs) have the capacity to fulfil the energy demand particularly for upcoming electric vehicle (EV) technology due to their high energy and power densities and safety. However, the technological success of ASSLBs heavily relies on developing fast lithium-ion conducting electrolyte materials the most critical component in terms of designing ASSLBs. In the present research, an attempt has been made to develop highly sintered LATP [$Li_{1+x}Al_xTi_{2-x}(PO_4)_3$] based material for its application as solid electrolyte in all solid-state lithium batteries.

LATP has been widely researched as solid-state electrolyte material due to its fast lithium ionic conductivity (10^{-5}-10^{-6} S/cm), wide potential window (0-6V) and high mechanical strength. Here, I have synthesized LATP material using solid-state synthesis method which is a top-down synthesis method and using XRD, FESEM, Archimedes principle (for density calculation of the sintered pellet of LATP), FTIR, TG-DTA for characterization studies and electrochemical studies include EIS (obtained result 10^{-4} S/cm) at AutoLab .

Charge discharge for both symmetric cell against Li-foil at ARBIN. We identified the interface stability of the material against Lithium metal which makes it a challenge for commercial use of the material in solid-state batteries. This has resulted in decrease in the interfacial resistance both at room temperature and at varied temperature from (30^o-120^o) C.

We have also studied the calendaring effect of the cell with LATP as solid- state electrolyte and lithium foil as on both side to check the stability and any chemical reaction occurring if exposed to atmospheric condition for long time.

INTRODUCTION

The development of solid electrolytes represents a significant advancement in the field of electrochemistry and energy storage technology. Traditional energy storage devices, such as lithium-ion batteries, typically employ liquid electrolytes to facilitate ion transport between the electrodes. While effective, liquid electrolytes present several drawbacks, including safety concerns, limited operating temperatures, and potential leakage issues. In recent years, there has been a growing interest in the exploration and development of solid electrolytes as alternatives to liquid electrolytes.

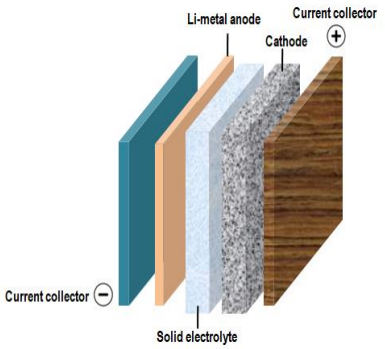
Solid electrolytes offer several advantages over their liquid counterparts. First and foremost, solid electrolytes provide improved safety characteristics, as they are non-flammable and less prone to leakage or thermal runaway events. This enhanced safety profile is particularly relevant for applications in high-energy-density batteries and electric vehicles, where safety concerns are paramount. Additionally, solid electrolytes exhibit a wider operating temperature range compared to liquid electrolytes, enabling reliable performance in extreme environments.

Furthermore, solid electrolytes offer the potential for increased energy density and enhanced electrochemical stability. By eliminating the need for a separator and reducing the volume occupied by the electrolyte, solid-state battery configurations can achieve higher energy densities. Moreover, solid electrolytes can suppress dendrite formation and improve cycle life, leading to more durable and long-lasting energy storage devices.

The development of solid electrolytes involves the exploration of various material classes, including ceramics, polymers, and composite materials. Each material class offers unique advantages and challenges, with researchers focusing on optimizing conductivity, mechanical strength, and compatibility with electrode materials. Advances in materials synthesis techniques, such as solid-state synthesis, thin-film deposition, and ion-conducting polymer fabrication, have enabled the creation of solid electrolytes with tailored properties for specific applications.

This introduction sets the stage for the exploration of the development of solid electrolytes from liquid electrolytes. By highlighting the advantages of solid electrolytes and the challenges associated with their development, it underscores the importance of ongoing research efforts aimed at advancing solid-state battery technology. Through interdisciplinary collaboration and innovative approaches, the transition from liquid to solid electrolytes promises to revolutionize the landscape of energy storage and contribute to the realization of a sustainable energy future.

CHAPTER-1

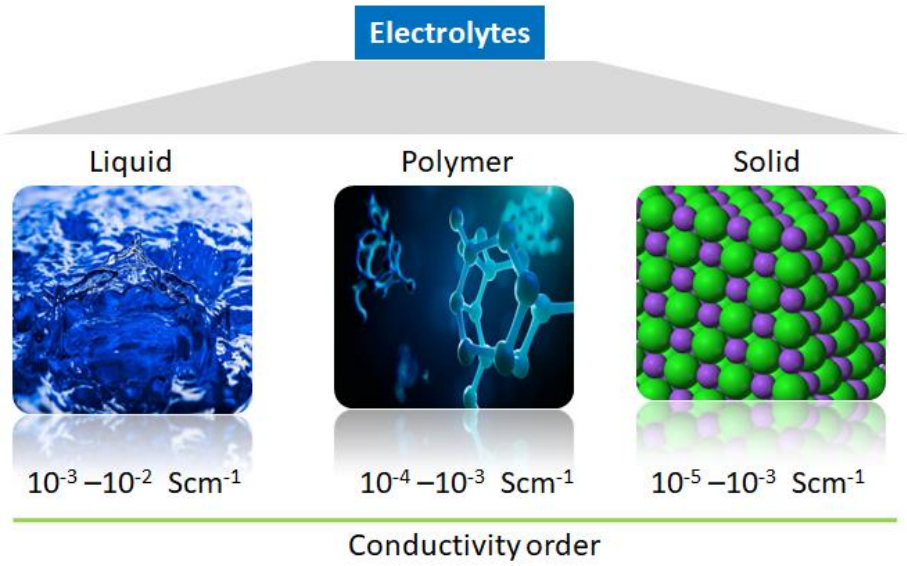


Prospect of Solid-State Lithium Metal Batteries (SSLMBs)

- **Electrolytes in Lithium Batteries - Liquid, Polymer and Solid**
- **Types of solids electrolyte (SEs)**
- **Solid polymer electrolytes (SPEs)**
- **Solid Composite electrolytes (SCEs)**
- **Inorganic ceramic electrolytes (ICEs)**

Evolution of electrolytes

(1990-2024)



Chapter 1

"This chapter traces the development of lithium battery electrolytes, progressing from liquid to polymer to solid states. It examines the assortment of electrolyte varieties employed in diverse lithium-ion battery (LIB) setups, offering a brief overview of each type, with particular emphasis on solid-state electrolytes (SSEs)"

Prospect of Solid-State Lithium Metal Batteries (SSLMBs)

Replacing liquid organic electrolytes with solid-state electrolyte (SSE) materials offers a viable solution to address safety concerns associated with current liquid electrolyte batteries. Moreover, this transition enhances the battery's energy density and ionic conductivity while reducing its weight. SSEs facilitate the use of high voltage cathodes and lithium metal anodes, enabling the creation of high-energy-density lithium batteries. They also mitigate dendrite formation, enhancing safety. Furthermore, SSEs offer advantages such as simplified design, leak-proof operation, reduced pollution, and improved resistance to shocks and vibrations compared to organic liquid electrolytes. Solid-state batteries primarily consist of three types of solid-state electrolytes: Solid Polymer Electrolytes (SPE), Inorganic Ceramic Electrolytes (ICE), and Solid Composite Electrolytes (SCEs).

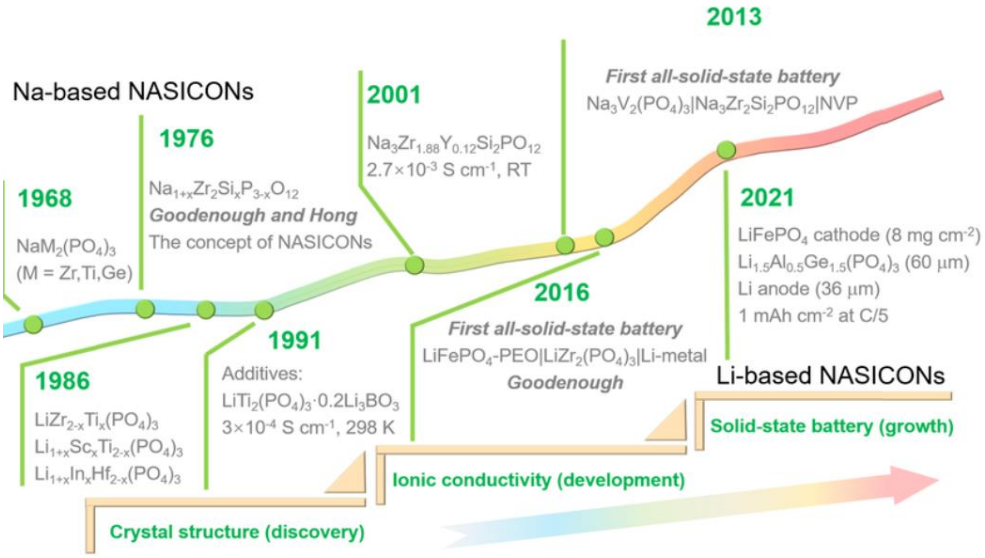


Figure 1: The history of NASICON superionic conductor solid-state electrolyte

1.1 Electrolytes in Lithium Batteries- Liquid, Polymer and Solid

'Electrolyte' – I will ensure a safe and swift journey for lithium ions! Here, we are delving into the transition from liquid electrolyte to solid-state electrolyte, exploring the pros and cons of each type along the way. Undoubtedly, ensuring electrochemical stability is merely one aspect of the criteria that an electrolyte must full fill. A comprehensive set of minimal requirements encompasses the following: (1) It must exhibit proficient ionic conductivity while maintaining electronic insulation to facilitate efficient ion transport and minimize self-discharge. (2) The electrolyte should possess a broad electrochemical window to prevent degradation within the operational potential range of both the cathode and the anode. (3) Additionally, it should demonstrate inertness towards other cell components, including separators, electrode substrates, and packaging materials. (4) Resistance to various forms of abuse, such as electrical, mechanical, or thermal stresses, is crucial. (5) Furthermore, its constituent materials should be environmentally sustainable [3]. A brief comparison has been given in the tabular column below.

Property	Liquid electrolyte	Polymer electrolyte	Solid electrolyte
Conductivity	10^{-3}-10^{-2} S/cm	10^{-4}-10^{-3} S/cm	10^{-5}-10^{-3} S/cm
Interfacial stability	Stable	Stable	Stability issue for both the electrodes
Thermal Stability	Poor thermal stability at high temperature [2]	Highly stable (~320°C)	Excellent thermal stability
Electrochemical stability window	~4.2V vs Li/Li^+	~ 4.6V vs Li/Li^+	~6V
Energy density	<300 Wh kg^{-1}	~400 Wh kg^{-1}	>500 Wh kg^{-1} [2]

Electrolyte Reactivity	Side reaction with cathode hence restrict cathode materials.	Low reactive	No Side reaction with cathode hence high voltage cathode materials can be used.
Fire safety	Highly flammable	Flammable	Non-Flammable
Production cost	Cost- effective	Cost effective	Costly

Table 1: Brief comparison among the electrolytes

1.1.1 Liquid Electrolytes in Lithium-ion batteries

At the outset, lithium-ion batteries (LIBs) typically consist of organic liquid electrolytes, graphite as the anode, and $LiCoO_2$ as the cathode, constituting the most prevalent battery type for portable electronics. The liquid electrolyte comprises of lithium salt, additives and solvent.[3] However, the use of organic liquid electrolytes poses significant safety risks due to their poor oxidation resistance, high flammability, and inadequate compatibility with lithium metal anodes. Commonly employed electrolytes in liquid electrolyte lithium batteries include LiB_6 and LiP_6, among others, with a notable propensity to form dendrites, potentially leading to short circuits.

Average ion mobility: $LiBF_4$ > $LiClO_4$ >$LiPF_6$ > $LiAsF_6$ > LiTf [3]

Dissociation constant: LiTf < $LiBF_4$ < $LiClO_4$ <$LiPF_6$ < $LiAsF_6$ [3]

- **Solvents**

(1) The electrolyte ought to have the capability to dissolve salts to a sufficient concentration, indicating a high dielectric constant (ε). (2) It should possess fluidity, characterized by low viscosity (η), facilitating smooth ion transport. (3) Maintaining inertness towards all cell components,

particularly the charged surfaces of the cathode and anode during cell operation, is imperative. (4) It must maintain a liquid state over a wide temperature range, implying a low melting point (T_m) and a high boiling point (T_b). (5) Safety considerations include a high flash point (T_f), non-toxicity, and cost-effectiveness.

Solvents	Advantages	Disadvantages
Carboxylates solvents	Low viscosity	Low dielectric constant
Carbonate solvents	High polarity, high dielectric constant	High viscosity, high intermolecular force, Slow lithium-ion movement
Carbonate and carboxylates solvents	Ensure battery safety, and improve the capacity retention rate and high-rate charge discharge capacity of low-temperature batteries	Strictly control water content and pay attention to solvation effect

Table 2: Brief comparison among the type of solvents in liquid electrolyte

- **Lithium salts**

For lithium-based batteries, the active nature of the strongly reducing anodes (such as lithium metal or highly lithiated (carbon) and the strongly oxidizing cathodes (composed of transition metal-based oxides) prohibits the use of solvents containing active protons, despite their effectiveness in solvating salts. This is because the reduction of such protons and/or the oxidation of the corresponding anions typically occurs within the range of 2.0-4.0 V [4] versus Li.

However, in current rechargeable lithium devices, the charged potentials of the anode and cathode generally range from 0.0-0.2 V and 3.0-4.5 V, respectively. On the contrary, nonaqueous compounds deemed suitable as electrolyte solvents must have the capacity to dissolve adequate amounts of lithium salt. Consequently, only solvents containing polar groups such as carbonyl (C=O), nitrile (C≡N), sulfonyl (S=O), and ether-linkages (-O-) are worthy of consideration.

Lithum salts	Advantages	Disadvantages
$LiPF_6$	With a suitable solubility and a higher ionic conductivity in the nonaqueous solvent; a stable passivation film can be formed on the surface of the aluminium foil concentration	Poor thermal stability, easy to decompose
$LiBF_4$	Width of the working temperature, good high-temperature stability, excellent low-temperature performance; enhance the film formation capability of electrolyte to electrodes, inhibiting aluminium foil corrosion	Lower ion conductivity
LiBOB	High electrical conductivity, wider electrochemical window, good thermal stability, better circulating stability, passivation protection of positive, or aluminium foil fluid	Low solubility
$LiAsF_6$	Have very high conductivity, stability, and battery charging discharge rate	Toxicity
LiDFOB	Good film formability, good low-temperature performance, is very well compatible with the positive pole of the battery, can form a passivation film on the surface of the aluminium foil, inhibiting electrolytic solution oxidation	Expensive
LiFSI	High electrical conductivity, low water sensitivity, and good thermal stability	Corroding aluminium foil when voltage 4.2 V
LiTFSI	Higher solubility and conductivity, thermal decomposition temperature exceeds 360 °C, not easy to hydrolyse.	Corroding aluminium foil when voltage is 3.7 V
$LiPF_2O_2$	Good low temperature performance; reduce battery interface impedance, improve the battery cycle performance.	Lower solubility
LTBP	Difficult to hydrolyse, good thermal stability, and high safety.	High molecular weight, high viscosity, and low conductivity

LiDFMFMB	Improve cycle stability and Coulomb efficiency	High molecular weight, high viscosity, and low conductivity
LiDFEFMB	Improve cycle stability and Coulomb efficiency.	High molecular weight, high viscosity, and low conductivity

Table 3: Brief comparison among the type of salts in liquid electrolyte

- **Additives**

  Electrolyte additives [5-9] constitute a category of substances that are added in minute quantities but can exert a significant positive impact on one or multiple properties of the battery. Functional additives represent the most cost-effective and efficient means of enhancing battery performance. By carefully selecting and adjusting the proportion of a small number of additives, the performance of electrolytes can be markedly enhanced. This has emerged as a central focus of research within the realm of lithium-ion battery electrolytes in recent years. Presently, there exist over 20 types of commercial additives, typically classified based on their functions into film-forming additives, electrolyte stabilizers, flame retardant additives, conductive additives, anti-overcharge additives, and various other additives.

Type	Classification	Effect
SEI forming additive	Inorganic film forming additive	Excellent SEI membranes have an organic solvent, allowing the liquid ion free access and exit electrode to prevent the solvent molecule to prevent the damage of the solvent molecule to the electrode, improve the cycle efficiency and reversible capacity of the battery
High ion conductivity additive	Organic film additive • Cationic type • Anionic Electrolyte ion type	Improve the dissolution and ionization of the conductive lithium salt and prevent the destruction of the solvent to the electrode

Flame retardant additive	-	Add some high boiling, high flash points, and non-flammable solvents to improve the safety of the battery
Overcharge protection additive		Adding a suitable redox pair in the electrolyte, this redox reduction is not participated in any chemical or electrochemical reaction at normal charging, and when the battery is filled with electricity or slightly higher than this value, the additive begins to oxidize on the positive electrode, and then diffuse into the reduction reaction occurs in the negative electrode.
Multifunctional additive	Boron-containing additive	Boron-containing compounds are often used as an additive to a lithium-ion battery of different positive electrode materials, during the battery cycle, many boron-containing compounds form a protective film on the surface of the positive electrode/electrolyte, thereby increasing lithium ions Battery performance
	Organic phosphorus additive	In addition to phosphite additives, the organophosphorus additives currently used include phosphate compounds. After a long cycle, it still maintains a very high capacity
	Carbonate additive	The fluorine-containing compound has a high electrochemical stability, and has hydrophobicity and oleophobic characteristics, forming a double-layer passivation film during the cycle, while reducing the degradation of the electrode, and the electrolytic solution. Oxidation decomposition.

Table 4: Brief comparison among the type of additives used in liquid electrolyte

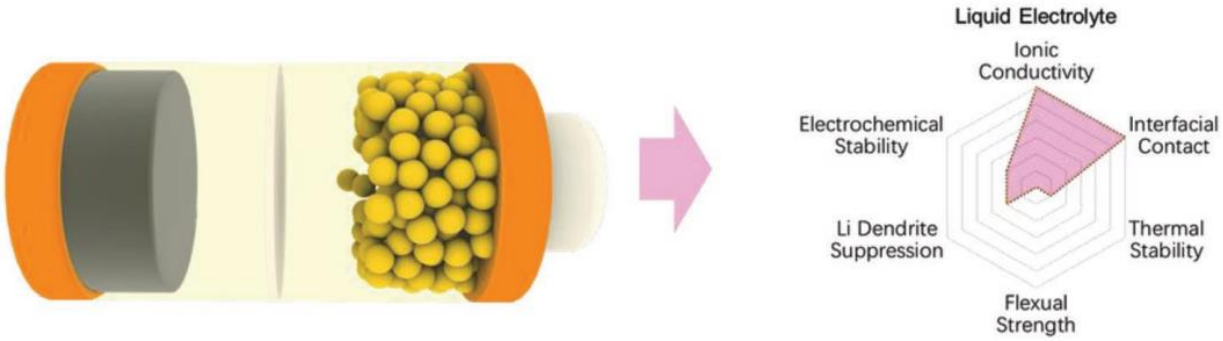


Figure 2: Schematic of Liquid electrolyte

1.1.2 Polymer Electrolytes in Lithium-ion batteries

Gel polymer electrolytes (GPE) have the characteristics of low fluidity, good flame retardancy, and interfacial compatibility, which can combine the advantages of both liquid electrolytes and polymer electrolytes. Replacing the liquid electrolyte with a polymer gel electrolyte is considered to be an effective solution to the current problems faced by LMBs. They present a promising alternative to liquid electrolytes with an ionic conductivity typically around 10^{-3} S/m at room temperature, these electrolytes offer solid-like flexibility. Their electrochemical window is broader, contingent upon the chosen solvent, facilitating excellent interfacial contact with electrodes.

Gel electrolytes predominantly employ polymeric networks, leveraging the mechanical strength afforded by high molecular weight. Additionally, their low glass transition temperature (-30°C) promotes rapid movement of polymer chains, while their high degradation temperature (500°C) ensures robustness.

Gel polymer electrolytes (GPEs) consist of a polymer backbone combined with a liquid organic electrolyte. Commonly used polymers in GPEs include polyethylene oxide (PEO) [10,11], poly (vinylidene fluoride-co-hexafluoropropylene) (PVDF-HFP) [12], polymethyl methacrylate (PMMA) [13], and polypropylene eyelet (PAN) [14]. Among these, PVDF-HFP stands out as a promising material due to its high dielectric constant, which enables exceptional room temperature ionic conductivity, superior mechanical strength, and electrochemical stability. However, the high crystallinity of PVDF-HFP often

results in suboptimal performance of the gel polymer electrolytes formed from it. To enhance GPE performance, researchers have introduced various inorganic fillers. These fillers can be categorized as inert or active inorganic electrolyte fillers. Active inorganic electrolyte fillers, such as Li0.33La0.557TiO3 (LLTO), Li7La3Zr2O12 (LLZO), Li10GeP2S12 (LGPS), and Li1.7Al0.3Ti1.7(PO3)4 (LATP), offer advantages over inert fillers like SiO2 and BaTiO3. They not only increase the amorphous area of the polymer matrix, facilitating lithium-ion transport, but also provide additional diffusion pathways for Li+. Among these, LATP, a NASICON-type fast ionic conductor, stands out for its exceptional room-temperature conductivity among oxide ionic fast conductors. Incorporating LATP into the polymer matrix increases the amorphous region, aiding lithium-ion transport. LATP's stability and wider electrochemical stabilization window.[15]

1.1.3 Solid Electrolytes in Lithium-ion batteries

The adoption of solid-state electrolytes (SSEs) in Solid State Batteries (SSBs) is seen as a solution to safety concerns, owing to their robust mechanical properties and electrochemical stability. SSEs offer a high energy density, and exhibit ionic conductivity at room temperature, typically around 10^{-4} S/cm for materials like LATP, which belongs to the NASICON structure family. Solid-state electrolytes can be categorized into several types based on their structures, including Solid Polymer Electrolyte (SPE), Inorganic Ceramic Electrolyte (ICE), and Solid Composite Electrolytes (SCEs). LATP serves as an example of an Inorganic Ceramic Electrolyte, specifically of the NASICON type.

1.2 Types of solids electrolyte (SEs)

Solid-state electrolytes (SSEs) offer advantages such as the absence of leakage or flammability, along with the ability to mitigate the formation of lithium dendrites in the anode. SSEs exhibit longer cycle lives and necessitate less packaging, facilitating the operation of higher series voltages compared to liquid electrolytes. Nonetheless, SSEs are still afflicted by certain limitations, including their intricate manufacturing procedures, inadequate mechanical resilience, and significant interfacial impedance. These issues persist as the primary challenges

impeding both the production and fundamental comprehension of SSEs. Solid electrolytes can be broadly classified into Solid polymer electrolytes (SPEs), Solid Composite electrolytes (SCEs), Inorganic ceramic electrolytes (ICEs). Based on the material used for the electrolyte the classification is done.

1.2.1 Solid polymer electrolytes (SPEs)

Solid Polymer Electrolytes (SPEs) offer numerous advantages: They are lightweight, flexible, possess excellent interfacial compatibility, and are highly processable. Crucially, they are also known for their safety. SPEs are produced by dissolving lithium salts within a high-molecular-weight polymer matrix. The polymer serves as a medium for the conveyance of lithium ions through the movement of polymer segments. Furthermore, solid polymer-based electrolytes are appealing because they can accommodate the volume fluctuations of electrodes through both elastic and plastic deformation. Consists of polyethylene oxide (PEO), Polyvinylidene fluoride (PVDF), polyacrylonitrile (PAN) and polyvinylidene fluoride hexafluoropropylene (PVDF-HFP) as copolymer matrix and for lithium-ion salt such as Lithium bis-trifluoromethanesulfonyl (Li TFSI), Lithium bis-fluorosulfonylimide (LiFSI) and Lithium perchlorate ($LiClO_4$).[16] Nonetheless, the ionic conductivities of SPEs fall short of the requisite conductivity threshold of 10^{-3} S/cm, thereby constraining their practical utility.

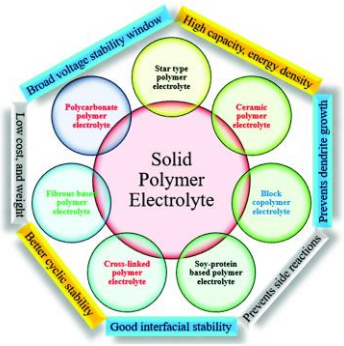


Figure 3: Different types of solid polymer-based electrolytes and their corresponding performances. (Ref. taken from: DOI: 10.1039/D2YA00043A (Review Article) *Energy Adv.*, 2022, 1, 457-510)

Few factors effecting the efficiency of the SPE which is explained below.

- **Ionic conductivity**

  In a Solid Polymer Electrolyte (SPE) setup, the Li^+ cations are dissolved within the polymer solvents and are mobilized through the movement of the polymer chains. The quantity of free Li^+ cations and the mobility of the chains play a significant role in determining the Li^+ transport capability within the SPE, consequently impacting battery performance. A comprehensive understanding of the conducting mechanisms is advantageous for designing and selecting polymer structures suitable for the room temperature operation of solid polymer lithium batteries. The conductivity (σ) of a material containing multiple conducting species is controlled by two factors: the quantity of charge carriers and their mobility. The conductivity can be expressed by Equation (1).

Equation (1)

$$\sigma = \sum n_i q_i \mu_i$$

In this context, n_i denotes the quantity of charge carriers of type i; q_i represents the charge of the charge carriers, and μ_i signifies the mobility. The ionic conductivity observed in SPE systems commonly adheres to two primary conduction mechanisms: either the Arrhenius equation or the Vogel-Tammann-Fulcher (VTF) equations, or a blend of both. [17,18]

The Vogel-Tammann-Fulcher (VTF) equation can be deduced from quasi-thermodynamic models incorporating considerations of free volume and configurational entropy. Its characteristics can be linked to the movement of ions in conjunction with the extensive motions of the polymer segments. This relationship can be formulated as follows:

Equation (2)

$$\sigma = \sigma_o T^{-1/2} \exp(-B/T-T_o)$$

- **Glass Transition Temperature (T_g)**

The glass transition temperature (Tg) stands as a pivotal property of polymers, marking the temperature at which chain segments initiate movement while the molecular chains themselves remain static. Below Tg, only molecular atoms or groups vibrate within their equilibrium positions, rendering polymers rigid and brittle with minimal molecular mobility. At Tg, a significant shift occurs in the physical characteristics of the polymer host, impacting density, specific heat, mechanical modulus, energy absorption, dielectric properties, acoustical behaviour, and the rate of diffusion for gases or liquids through the polymer. Typically, Tg is determined through measurements using techniques like differential scanning calorimetry (DSC), with factors such as polymer structure, crystallinity, molecular weight, thermal history, and pressure influencing its value. Lowering Tg generally increases the mobility of polymer chains, thereby enhancing ionic conductivity, which is crucial for Solid Polymer Electrolytes (SPE). Above Tg, ions can move within the space provided by the polymer host's free volume, migrating between coordination sites along the chains or hopping from one chain to another under an electric field. Given the typically low Li-ion conductivity in SPE at room temperature, strategies have been devised to reduce Tg and enhance conductivity. These include incorporating branched chains with lower Tg values compared to the host polymer chain and introducing nano-additives, both of which effectively improve ion transport capabilities in SPE.

- **Degree of crystallinity**

Crystallinity refers to the degree of long-range order within a material and plays a crucial role in determining its properties. In polymers, crystallization occurs as molecular chains partially align, a process influenced by factors such as cooling from a melt or solvent evaporation

during film fabrication for polymer electrolytes. Besides crystallinity, properties are influenced by the size and orientation of molecular chains. Methods like density measurements, DSC, XRD,[19] infrared spectroscopy, and NMR are used to estimate crystallinity, while techniques like polarized light microscopy and transmission electron microscopy visualize the distribution of crystalline and amorphous regions. The crystallization process involves nucleation and crystal growth, starting with small nucleation seeds where molecular chains align and subsequently grow. Nucleation is influenced by impurities, plasticizers, fillers, and additives, which can reduce crystallinity. SPE membranes are typically manufactured using solvent casting or hot-press filming methods, each affecting crystal growth differently between the melt and solution phases.

Criteria of a polymer for SPEs

- Solubility: Sequential polar groups like -O-, C=O, and C≡N are necessary to dissolve lithium salts and create polymer-salt complexes.
- Electrochemical Stability: A broad voltage window with significant gaps between onset potentials for oxidation and reduction decomposition is essential.
- Ionic Conductivity and Insulation: High ionic conductivities, ion transference numbers, and electrical insulation are required to maintain performance and minimize self-discharge, ensuring prolonged storage life.
- Chemical and Thermal Stability: Absence of chemical reactions during battery operation, including interactions with electrodes, current collectors, and packaging materials, along with robust thermal stability for safety.
- Mechanical Strength: Strong dimensional stability is crucial for processing feasibility and isolating positive and negative electrodes.

- Furthermore, for large-scale applications, SPEs must meet practical criteria such as affordability, sustainability through the use of abundant elements and environmentally friendly synthesis, and low toxicity to minimize pollution and environmental hazards.

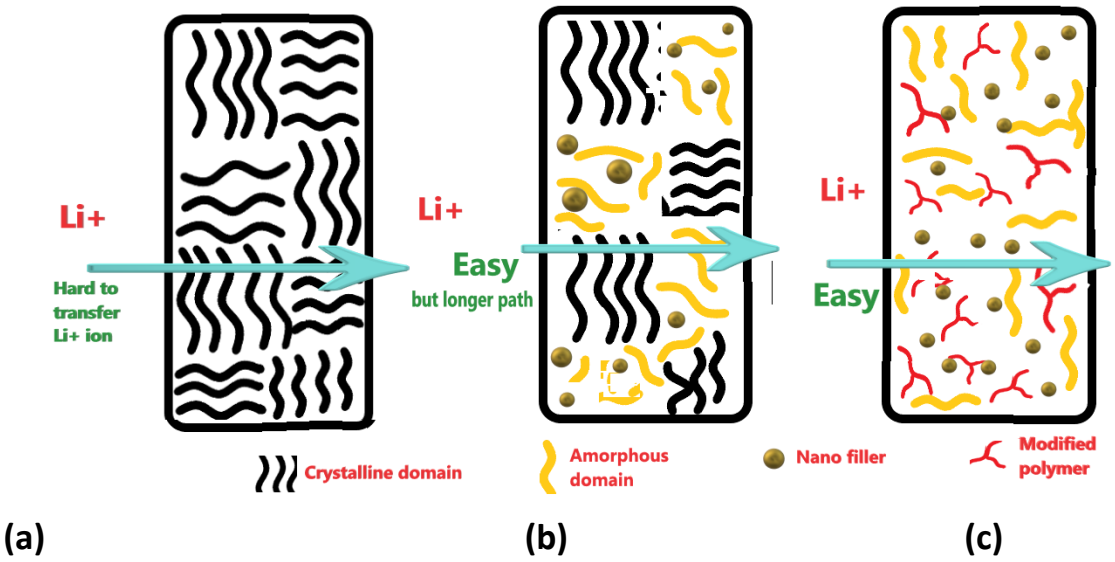


Figure 4: Schematic illustration of the lithium-ion transfer across (a) a crystalline polymer, (b) crystalline polymer with nanofillers, and (c) modified polymer with nanofillers

1.2.2 Solid Composite electrolytes (SCEs)

Solid electrolyte composites typically comprise a solid electrolyte matrix, which could be ceramic or polymer-based, along with different additives or dopants aimed at altering its characteristics. These additives may involve conductive fillers like carbon nanotubes or metallic particles to boost electrical conductivity, as well as inert substances to enhance mechanical strength or stability. Such composites exhibit notable ionic conductivity and establish effective interfacial contact with the electrode. Examples of solid composite electrolyte designs include combinations like inorganic nanoparticle/polymer, inorganic nanofiber/polymer, and various other inorganic/polymer composite solid electrolytes. Solid Composite Electrolytes (SCEs) that combine Solid Polymer

Electrolytes (SPEs) with inorganic fillers amalgamate the benefits of both components. These SCEs offer high ionic conductivity (>10^{-4} S/cm), excellent flexibility, and close contact with electrodes. Consequently, SCEs are viewed as highly promising electrolyte options for future all-solid-state lithium batteries.

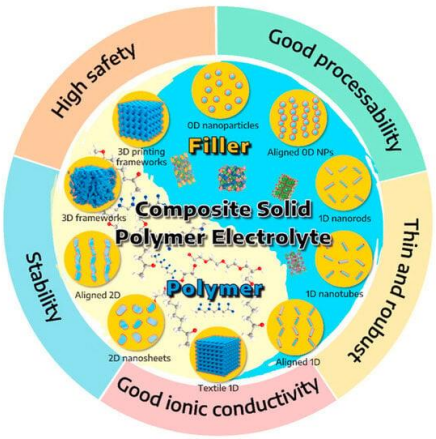


Figure 5: Illustration depicting the structure of fillers and template polymers used in developing CSEs. The graphic also highlights the overarching benefits of using CSEs. [2] (Ref. taken from Nguyen, A.-G.; Park, C.-J. Insights into Tailoring Composite Solid Polymer Electrolytes for Solid-State Lithium Batteries. *J. Member. Sci.* 2023, *675*, 121552)

1.2.3 Inorganic ceramic electrolytes (ICEs)

- NASICON type=$Li_{1+x}Al_xTi_{2-x}(PO_4)_3$, $Li_{1+x}Al_xGe_{2-x}(PO_4)_3$
- LISICON type=$Li_{1+x}Zn_{1-x}GeO_4$
- Garnet type=$Li_7La_3Zr_2O_{12}$
- Perovskite-type=$Li_{0.34}La_{0.51}TiO_{2.94}$
- Sulfide based=LiPON

The ionic conductivity is mainly determined by the transfer mechanism. In the phase of bulk ICEs, the Li ion transfer mainly depends on the motion of vacancies or interstitial ions that results in fast ion conduction, while the migration of ions in polymer matrix under an electric field is related to the breaks/formations of coordination bonds during the local segmental motions of polymer chains, which mainly occurs in the amorphous sections.[20,21]This electrolyte offers

significant advantages such as high room temperature conductivity, strong resistance to voltage oxidation, and impressive mechanical durability. However, a notable drawback of this electrolyte is that ceramics, which are part of its composition, tend to be brittle and inflexible, leading to suboptimal contact with the electrodes. Among, the various types mentioned, LATP of the NASICON type stands out for its superior ionic conductivity, ranging from 10^{-4} to 10^{-3} S/m. Additionally, it boasts good chemical stability and a high oxidation voltage of 6V. Moreover, LATP is commercially advantageous due to its lower raw material costs.

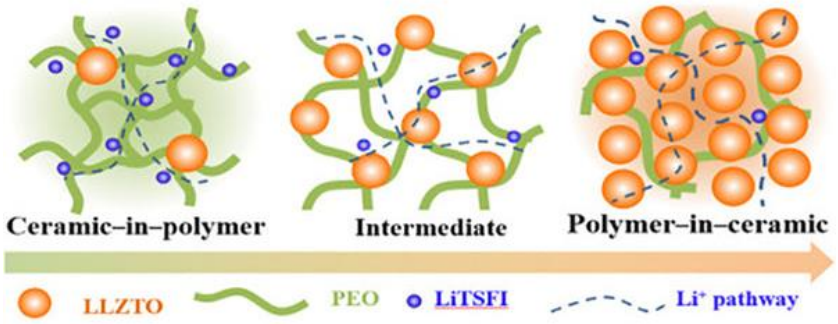


Figure 6: Illustration of Inorganic ceramic polymer as electrolyte

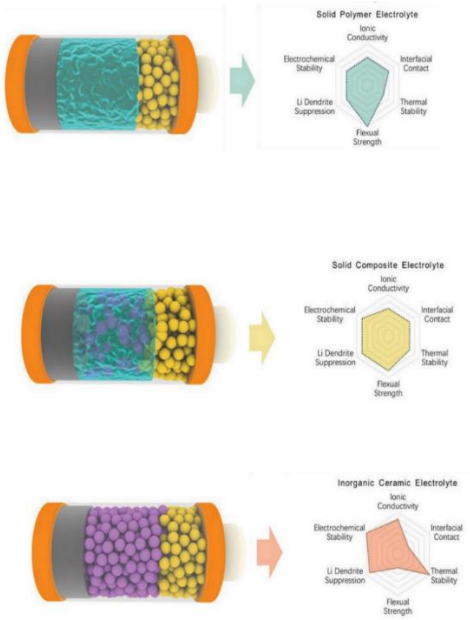
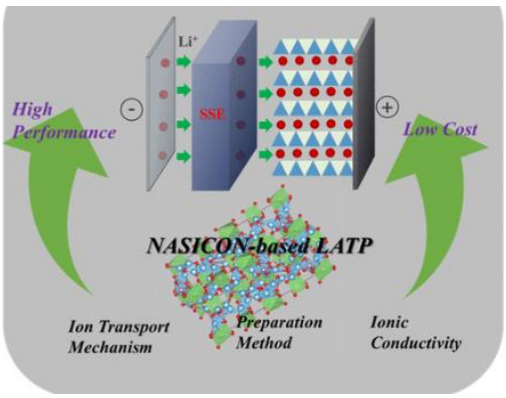


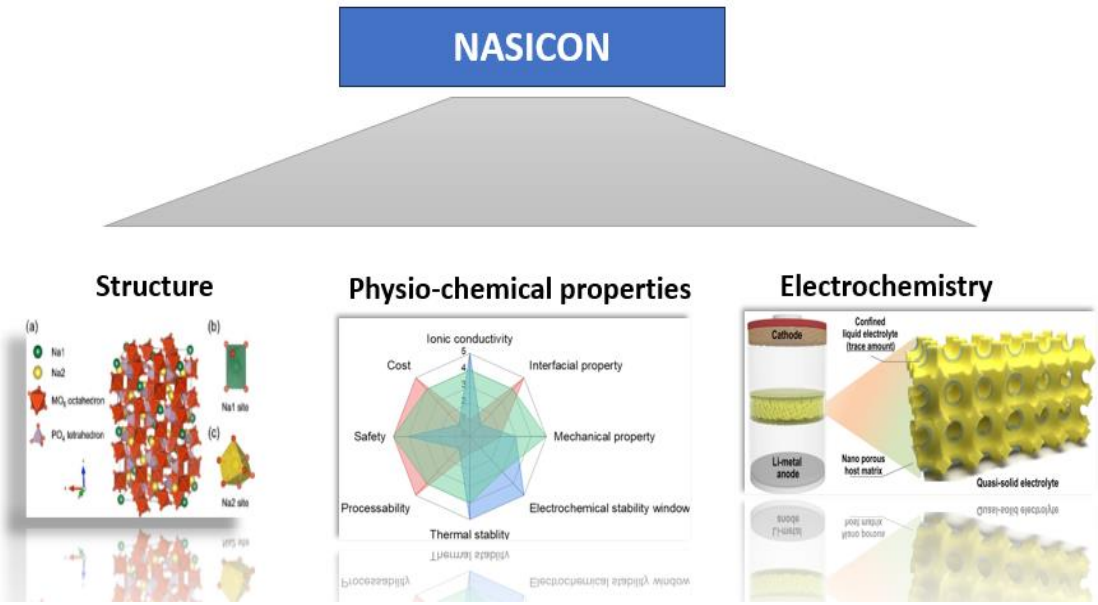
Figure 7: Comparisons of types of solid electrolytes (a) SPE (b) SCE (c) ICE

CHAPTER-2



Crystalline electrolytes & NASICONs and $LiA_2^{IV}(PO_4)_3$ [A^{IV}: Ti, Zr, Ge, Hf]

- Crystalline electrolytes: LISICON, Thio-LISICON, Garnet, Perovskite, NASICON
- Glass based electrolytes
- Glass-ceramic based electrolytes
- Structure of NASICON
- Physio-chemical properties of NASICON
- Electrochemistry of NASICON in SSLMBs



Study of NASICON structure as solid-state electrolyte

Chapter 2

"This chapter traces the study of other electrolytes such as glass based. Focusing on structural, physio-chemical and electrochemistry of NASICON as solid-state electrolyte. The development of NASICON structure which was discovered for Na^+ and later converted into Li^+ conductor".

2.1 Crystalline electrolytes, glass and glass-ceramic based electrolytes

Crystalline electrolytes include LISICON and thio-LISICON type, Perovskite-type, Garnet type, and NASICON type lithium-ion conductors. Here, LISICON produce low conductivity of 10^{-7} S/cm at room temperature. It is usually represented as $Li_{2+2x}Zn_{1-x}GeO_4$.

Whereas glass-based electrolytes have no grain boundary resistance so ionic conductivity is also becomes high in this case. Ease, of fabrication and drawn into film. In this case type ionic conductivity of amorphous glass is more than that of crystalline glass.

2.1.1 Crystalline electrolytes: LISICON, Thio-LISICON, Garnet, Perovskite, NASICON

Conductivity of LISICON type solid electrolyte is low at room temperature (~10^{-7} S/cm). The generalised formula for LISICON can be written as $Li_{2+2x}Zn_{1-x}GeO_4$.This can be imagined as a solid solution of Li_4GeO_4-Zn_2GeO_4 .$Li_{14}ZnGe_4O_{16}$ is highly reactive with atmospheric CO2 and Li-metal resulting in the decrease in conductivity. The ionic conductivity can be increased by replacing the oxide by sulphur in the LISICON structure resulting in Thio-LISICON. Few materials design basic structural criteria should be followed are (i) conduction pathways should be large in lattice for mobile ions (ii)there should be a disorder mobile-ions in sublattice (iii)highly polarizable mobile ions and anion sublattice are preferred.

Sulphur has higher radius than Oxygen atom resulting in the enlargement of the Li+ transport bottlenecks. Sulphur also had better polarization capability than

Oxygen which weakens the interaction between Li+ ions and skeleton. Thus thio-LISICON structure has high ionic conductivity (~10^{-4} S/cm) at room temperature. It has less grain boundary resistance.

General formula for Garnet type electrolyte is $Li_5La_3M_2O_{12}$ (M=Ta, Nb). Higher ionic conductivity and chemical stability in contact with lithium metal. M occupy the six coordinate and Lanthanum occupy eight site and Lithium occupy the octahedral sites. One of the garnet type electrolytes is $Li_7La_3Zr_2O_{12}$(LLZO). Reported, studies have shown $Cu_{0.1}V_2O_5$/LLZO/Li all solid-state battery exhibited an initial discharging capacity of 93mAh/g at 10micron A/cm^2 at 50^{o}C.

The Lithium lanthanum Titanate (LLTO) with a perovskite structure (ABO3) whose ionic conductivity at room temperature is (~10^{-3} S/cm). LLTO consists of both high temperature phase and low temperature phase. Advantages of LLTO as electrolyte is negligible electronic conductivity, high electrochemical stability(>8V) and lithium single ion conductors. But disadvantages is low grain boundary ionic conductivity (<10^{-5} S/cm) and instability against Li metal anode.

NASICON type electrolyte stands for Na+ super ionic conductors were first solid solution phase $Na_{1+x}Zr_2Si_xP_3$-xO_{12}, x=2.0. General formula for NASICON $LiA_2^{IV}(PO_4)_3$ [A^{IV}: Ti, Zr, Ge, Hf]. Maximum ionic conductivity has been found in $LiTi_2(PO_4)_3$. An increase in ionic conductivity was found in when the Ti^{4+} was partially replaced by Al3+ where the general formula becomes $Li_{1+x}Al_xTi_{2-x}(PO_4)_3$. and conductivity at room temperature is 3x10^{-3} S/cm.

2.2.2 Glass based electrolytes

Milling techniques in order to make good contact with the electrode. Advantages of this process is it can be performed at room temperature and forms amorphous materials.

2.2.3 Glass-ceramic based electrolytes

Glass ceramic electrolyte can be formed by the crystallization of the precursor material. The crystallization usually decreased the ionic conductivity but the precipitation of superionic conducting crystal from a precursor can enhance the ionic conductivity. The grain boundaries in the crystal domains are filled with the

amorphous phase. This results in the lower grain boundary resistance than polycrystalline system. Again, the Glass-ceramic electrolyte can be classified into oxide based and sulphur based. The most studied oxide-based glass-ceramic electrolyte is NASICON based example is LATP and LAGP. Ionic conductivity of them can reached 10^{-3}-10^{-4} S/cm. Sulphide based glass ceramic has higher ionic conductivity due to its large ionic radius and high polarizibility. Ionic conductivity of Li2S-P2S5 glass ceramic can reach 10^{-3} S/cm at room temperature.

Recently a thio-LISICON was reported with high ionic conductivity at room temperature $1.7x10^{-2}$ S/cm by optimizing the heat treatment resulting in the reduction of grain boundary resistance thus resulting in the increase of ionic conductivity by 5times.

2.2 NASICONs and $LiA_2^{IV}(PO_4)_3$ [A^{IV}: Ti, Zr, Ge, Hf]

NASICON structure was first discovered in Na^+ conductor of $NaM_2(PO_4)_3$ where (M=Ge, Zr). This NASICON structure consists of PO_4 tetrahedra and MO_6 octahedra. The structure consists of 2 MO_6 octahedra and 3 PO_4 tetrahedra connected by the top oxygen atoms forming a 3D structure of Na^+ transporting networks .When the substitution of Na^+ and M sites are done by Li^+ and Ti^+ atoms ,the material is primary NASICON structure but converts into Li^+ conductor LTP that is $LiTi_2(PO_4)_3$.The main issue with LTP is it has poor conductivity at room temperature .To overcome this either iso-valent or aliovalent substitution can be used. But adding iso-valent substitution which has larger atomic size than Titanium increases the size of lithium transport pathways and lower the activation energy. Whereas for aliovalent substitution, the ionic conductivity is enhanced due to its Li^+ concentration is increased.

2..2.1 Structure and physio-chemical properties

NASICONs, short for Sodium (Na^+) Super Ionic Conductors, comprise a class of superionic conductors known for their unique 3D interstitial structure, allowing for high ionic conductivity. These materials have gained substantial attention in the realm of solid-state electrolytes and energy storage due to their exceptional ionic conductivity, expansive potential range, and wide operational temperature scope. Let's break down the information in a rephrased manner: General

Formula: NASICONs have a general formula represented as $AMM'P_3O_{12}$ or $AMM'(PO_4)_3$. Here, "A" can denote a variety of cations, such as Li^+, Na^+, K^+, Rb^+, Cs^+, Mg^{2+}, Ca^{2+}, Sr^{2+}, Ba^{2+}, H^+, H_3O^+, NH_4^+, Ag^+, and more. "M" and " M' " can be filled with various metal ions, like Zn^{2+}, Sc^{3+}, Al^{3+}, Y^{3+}, Zr^{4+}, Si^{4+}, Ta^{5+}, Nb^{5+}, and others. Additionally, "P" can be partially substituted by Si to facilitate the movement of A cations while maintaining charge balance.

NASICONs can take on various crystal structures, including rhombohedral, monoclinic, triclinic, and others. The most prevalent is the rhombohedral structure, characterized by a 3D framework comprised of M(M') O_6 octahedra and PO_4 tetrahedra with shared oxygen corners. This framework creates interconnected channels and spaces, enabling the mobility of conducting A cations. Two types of "A" sites, A1 and A2, are found within the crystal structure.

The ease with which A cations move within NASICONs depends on the size of "constriction points" in the pathways they must traverse. These constriction points must be larger than the diameter of the mobile ions to facilitate ion transport. The size and quantity of these constriction points can impact the energy barrier for ion migration.

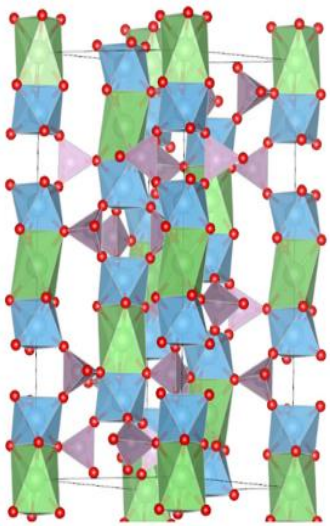


Figure 8: Crystal structure of NASICON type solid electrolyte. Red spheres are oxygen ions; greens are lithium ions; blue spheres are titanium ions; violets are phosphorous ions. (For interpretation of the references to colour in this figure legend, the reader is referred to the web version of this article.) Reference has been taken from N. Tolganbek et al. / Materials Today: Proceedings 25 (2020) 97–100

NASICONs are especially captivating as solid-state electrolytes, particularly in situations where readily available redox metals are absent. These materials offer several benefits, including outstanding ionic conductivity, a broad range of potential windows, and a wide operating temperature span. Their potential for advanced energy storage systems, such as solid-state batteries are being explored. In recent years, there has been notable advancement in the research and understanding of NASICONs as solid-state electrolytes.

LATP is chemically stable in humidified air or carbon dioxide [22] and is expected to exhibit a high oxidative potential (4.21 V) compared to LiPON (2.63 V) or garnet-type electrolytes (2.91 V) [23]. In recent years, LATP has attracted significant attention as a promising solid electrolyte for all-solid-state lithium batteries.

Table 5: Properties of NASICON

Properties of LTP (NASICON type)	Values of the specifications of LTP
Hardness	3GPa (applied load of 30 mN) [24]
Theoretical Density	2.92 g/cc [25]
Ionic conductivity at RT	8.04×10^{-5} S cm^{-1} [26]
Activation Energy	0.37eV [27]
Electrochemical window	1.85–4.9 V [28]
Safety	Non-flammable

2.2.2 Electrochemistry of NASICON in SSLMBs

In the NASICON family of materials, the migration of Na^+ ions depend on a process of hopping from one site to a nearby vacant site, which involves passing through a triangular area formed by three oxygen atoms. This triangular region, referred to as the 'bottleneck,' is a crucial factor in determining the energy barrier for ion migration and, consequently, impacts the material's ionic conductivity. The size of this bottleneck is of paramount importance because it directly affects the energy barrier for ion migration. A larger bottleneck area

reduces this energy barrier, making ion diffusion easier and thereby enhancing the material's ionic conductivity.

By substituting Zr^{4+} with elements such as Mg^{2+}, Sc^{3+}, and Ga^{3+}, it is possible to increase the bottleneck area in the monoclinic NASICON structure. This substitution leads to larger bottleneck areas compared to the original material, resulting in improved ionic conductivity.

Moreover, the occupancy of Na sites also influences the behavior of Na^+ ion transport. Substituting Zr^{4+} with a lower valent dopant leads to the preferential occupation of higher energy sites by introduced Na^+ ions, reducing the energy barrier for ion migration. However, excessive occupation of these sites can lead to increased Columbic repulsion among cations, potentially promoting correlated migration and Na^+ ion diffusion up to a point where the Na sub-lattice becomes overcrowded.

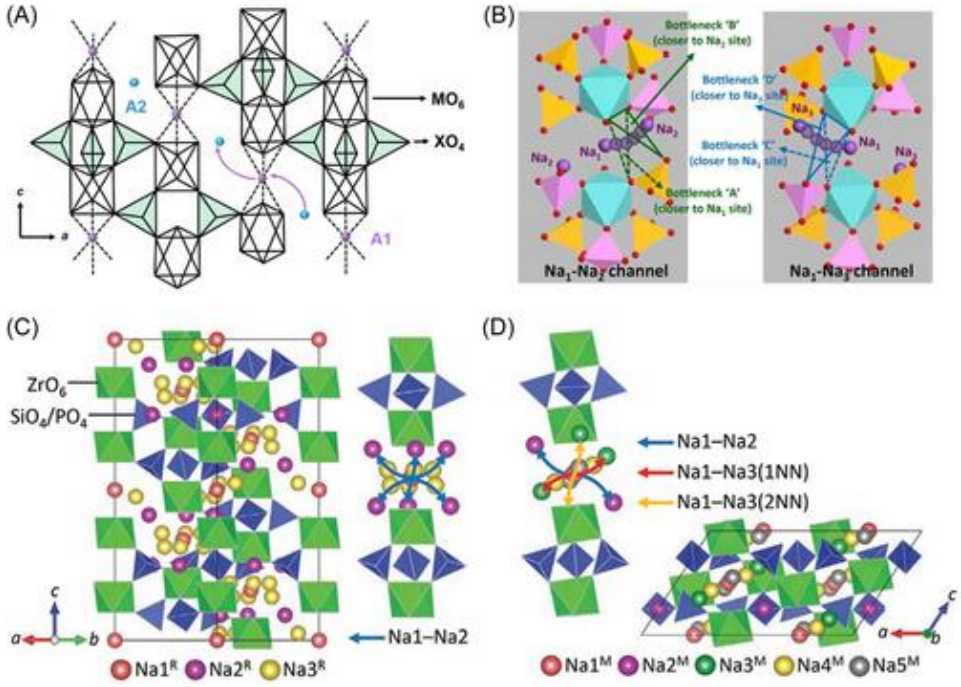
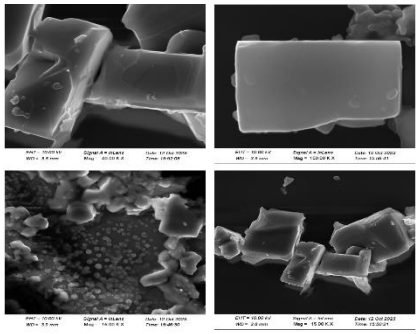


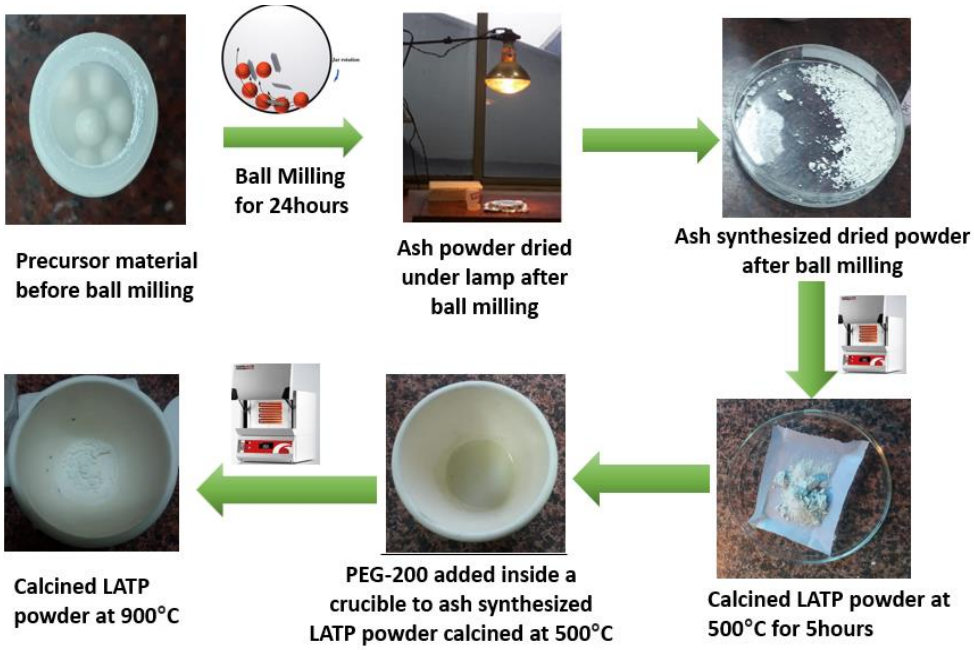
Figure 9:(A) The rhombohedral structure showing A1 and A2 sites; (Ref.Springer Science+Business Media, LLC 2011); (B) the different bottlenecks of monoclinic sodium superionic conductors structure; (copyright 2016 American Chemical Society); the unit cells and Na^+ migration channels (C) rhombohedral; and (D) monoclinic $Na_3Zr_2Si_2PO_{12}$.(Ref copyright 2021 Wiley-VCH GmbH).

CHAPTER-3

Studies on LATP: $Li_{1.5}Al_{0.5}Ti_{1.5}(PO_4)_3$



- Synthesis of LATP (Ball- milling)
- Structural and Microstructural properties
- Thermal Analysis of the microstructure
- Density Calculation of the material by Archimedes principle



Study of LATP as solid-state electrolyte

Chapter 3

"This chapter traces the study of LATP solid state electrolyte. Starting from its synthesis from precursor, characterization of the powder and its electrochemical studies. Symmetric cell study of the symmetric cell has been done along Lithium foil on both sides."

3.1 Synthesis

LATP is primarily synthesized using the ball milling method, a top-down synthesis approach. This solid-state synthesis is typically used for oxides and carbonates. Calcination at high temperatures is performed to achieve a homogeneous solid mixture. In our solid-state synthesis process described below, PEG-200 is used as a sacrificial material.

Equipment used

- Ball mill
- High Accuracy Electric Weight Balance
- Vacuum oven (Carbolite gero 30-3000C)

Materials used

- Lithium carbonate (Li2CO3) by ACROS Organics (99% pure)
- Aluminium Oxide (Al2O3) average particle size <=10micrometer by Sigma-Aldrich (99.9% pure)
- Titanium (IV Oxide (TiO2) anatase powder by ACROS Organics (98% pure)
- Ammonium dihydrogen phosphate (NH4H2PO4) by ACROS Organics (99.99% pure)
- Iso-Propyl Alcohol (IPA)
- Polyethylene Glycol 200 (PEG-200)
- Deionised Water



Figure 10: Reagents used for the synthesis of LATP

Procedure

An initial batch of 2 grams of the resultant material was prepared. Stoichiometric amounts of the precursor were ball-milled with isopropyl alcohol for 24 hours at 150 rpm using zirconium balls. After milling, the mixture, along with the zirconium balls, was placed in a petri dish and dried under a lamp. Calcination was performed at 500°C for 6 hours. Following calcination, a portion of the sample was set aside for microstructural studies. The remaining sample was weighed. It was then crushed using a mortar and pestle, reducing the weight. PEG-200 was added at 5% wt. along with IPA to this sample. The mixture was ball-milled again for 18 hours at 150 rpm with zirconium balls. The resultant mixture was transferred to an alumina crucible and heated under lamp to remove excess IPA. Finally, it was calcined again at 900°C for 25 hours, with a dwell time of 10 hours and a temperature increase rate of 2°C per minute.

The figure below shows that the LATP+PEG sample is not completely dried due to the presence of polyethylene glycol polymer. The sample was placed under a lamp to evaporate any remaining isopropyl alcohol (IPA) present in the sample. The figure below shows the LATP sample after being calcined for 10 hours at 900°C in an alumina crucible. The powder obtained after grinding this sample was much smoother and finer compared to the sample calcined at 500°C.

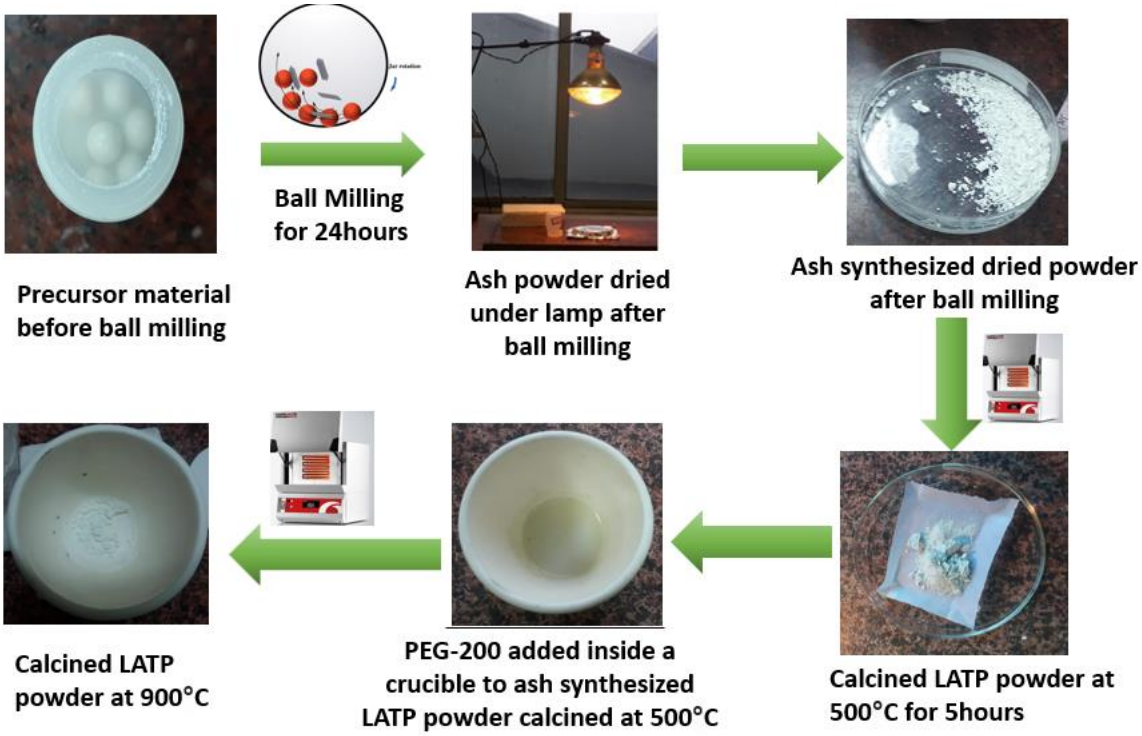


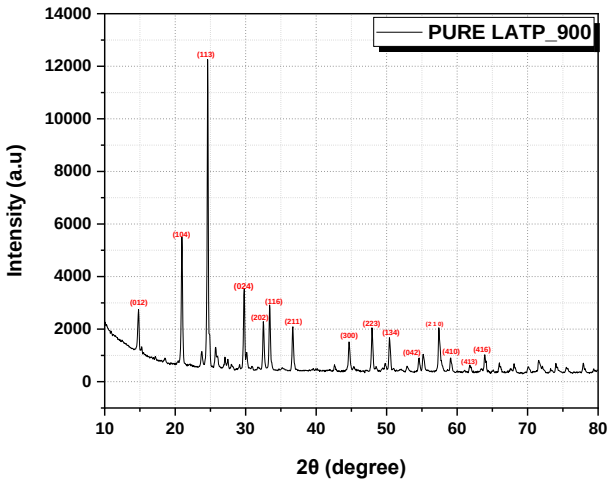
Figure 11: Synthesis process of LATP solid electrolyte by ball milling

3.2 Structural and Microstructural properties

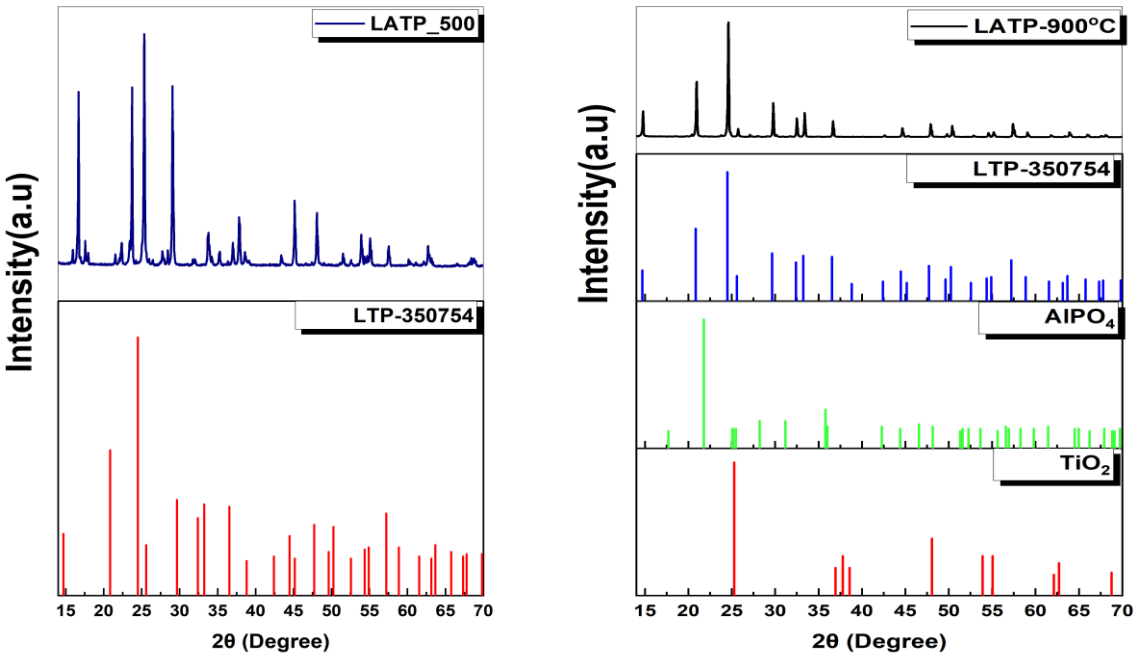
➢ 3.2.1 XRD Analysis

X-ray diffractograms were collected using an X'pert Pro MPD XRD system (PANalytical, Netherlands) with nickel-filtered Cu Kα (λ= 1.5406Å) radiation and irradiated at 40 kV and 40 mA with a step size of 0.02 to investigate the purity of phases present in the LATP powder. XRD pattern of the powder prepared by solid state synthesis are shown in the figures. The synthesis detail has been mentioned in the synthesis section. The standard diffraction peaks of the $LiTi_2(PO_4)_3$ have been showed in the figure. JCPDF card no. 00-035-0754.NASICON type LATP formed has been confirmed from the XRD graph. XRD of both the sample where calcination was done at 900C and 500C was done. A single phase LATP at 900°C without any impurities being formed. The PDF from X'pert HighScore has been used to match the impurities data with our XRD data to trace any impurities

formed during calcination or not. JCPDF number for LTP is 00-035-0754, $AlPO_4$ is 00-011-0500 and TiO_2 is 00- 021-1272.



(a)



(b) (c)

Figure 12:(a) XRD graph plotted for pure LATP calcined at 900°C (b)LATP plotted with LTP data #PDF-350754 confirming the formation of LATP powder. (c) XRD of LATP powder formed plotted along LTP(#PDF-350754) along with probable impurities that might form $AlPO_4$, TiO_2

The graph above is from a sample of LATP calcined at 500°C for 5 hours, with a temperature increase of 2°C per minute in the furnace. The graph in the figure demonstrates the successful synthesis of NASICON-type LATP with x = 0.5 within the temperature range of 500 to 900 degrees Celsius during calcination. This finding indicates that specific conditions calcination temperatures in this range lead to the successful formation of the desired material

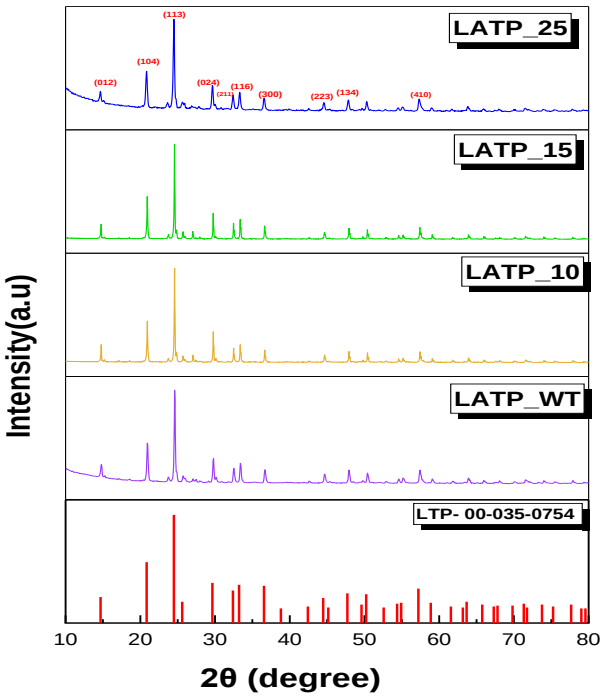


Figure 13: XRD data of pure LATP and various concentration of PEG-200 added during the 2nd calcination at 900°C of the LATP initially calcined at intermediate temperature of 500°C

Now, partially Titanium has been dopped with Aluminium resulting in LATP formation. The addition of PEG in the 2nd calcination step has not changed the material or no formation of impurities as per the graphs seen. But later we can see the change in morphology due to the addition of various concentration of PEG and other electrochemical parameters.

➢ 3.2.2 Field Effect Scanning Electron Microscopy (FESEM)

❖ Sample Mounting

A small amount of the specimen is placed in a test tube, and then acetone is introduced to the sample. The particle is dissolved and evenly spread out by subjecting it to ultrasonic waves for 15 minutes. On a sample holder shaped like the letter 'T', double-sided tape is affixed, and two extremely tiny glass slides are positioned on the tape. Using a micro-pipette, a small droplet of the specimen is applied to the slide. The glass slide is then dried using an infrared (IR) lamp until a hazy appearance becomes apparent on the surface.

❖ Morphology Analysis

Once the mounting was completed we send the sample for imaging under FESEM. The microstructure and morphology of the pristine LATP and PEG added LATP samples were analyzed using a scanning electron microscope (SEM, Phenom TM, Model Pro-X, USA) and field emission scanning electron microscope (FESEM, SupraVP35 Carl Zeiss, Germany). The below images can be seen of LATP calcined at 500^{o}C for 5hours that is the first step calcination of LATP sample. Here a cubic shape structure can be seen. In the second image figure we can see a blunt cubic structure of the sample where 5% PEG is added and a further 2nd step calcination was done for 10hours at 900^{o}C. From the final calcined image of LATP we can see a spherical agglomerated sample. Qualitative analysis in EDX has been done for both the samples. Impurities that have been found in the graph can be from the IPA or Acetone used while ultrasonication or during ball milling.

We can confirm the presence of Aluminium, Phosphorous, Titanium, Oxygen from the graph in EDX.

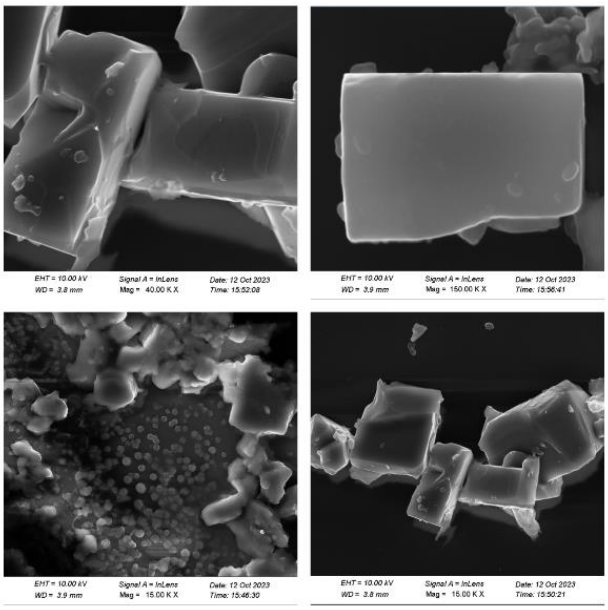


Figure 14: FESEM images for LATP calcined at 500°C

We have done FESEM analysis of the intermediate calcined LATP powder which was calcined at 500°C for 5 hours. This morphology confirms the partial formation of LATP along with the presence of spherical particles which confirms the presence of intermediate phase other impurities that might be present inside the sample due to the use of IPA while ball milling.

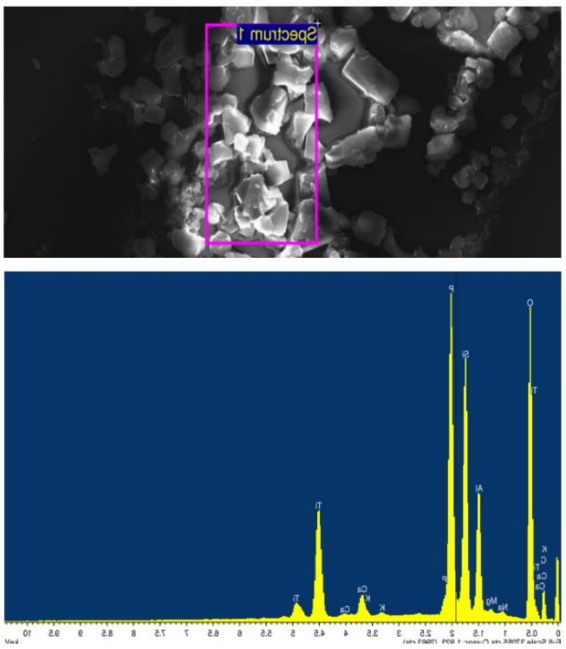


Figure 15: EDX of LATP calcined at 500°C

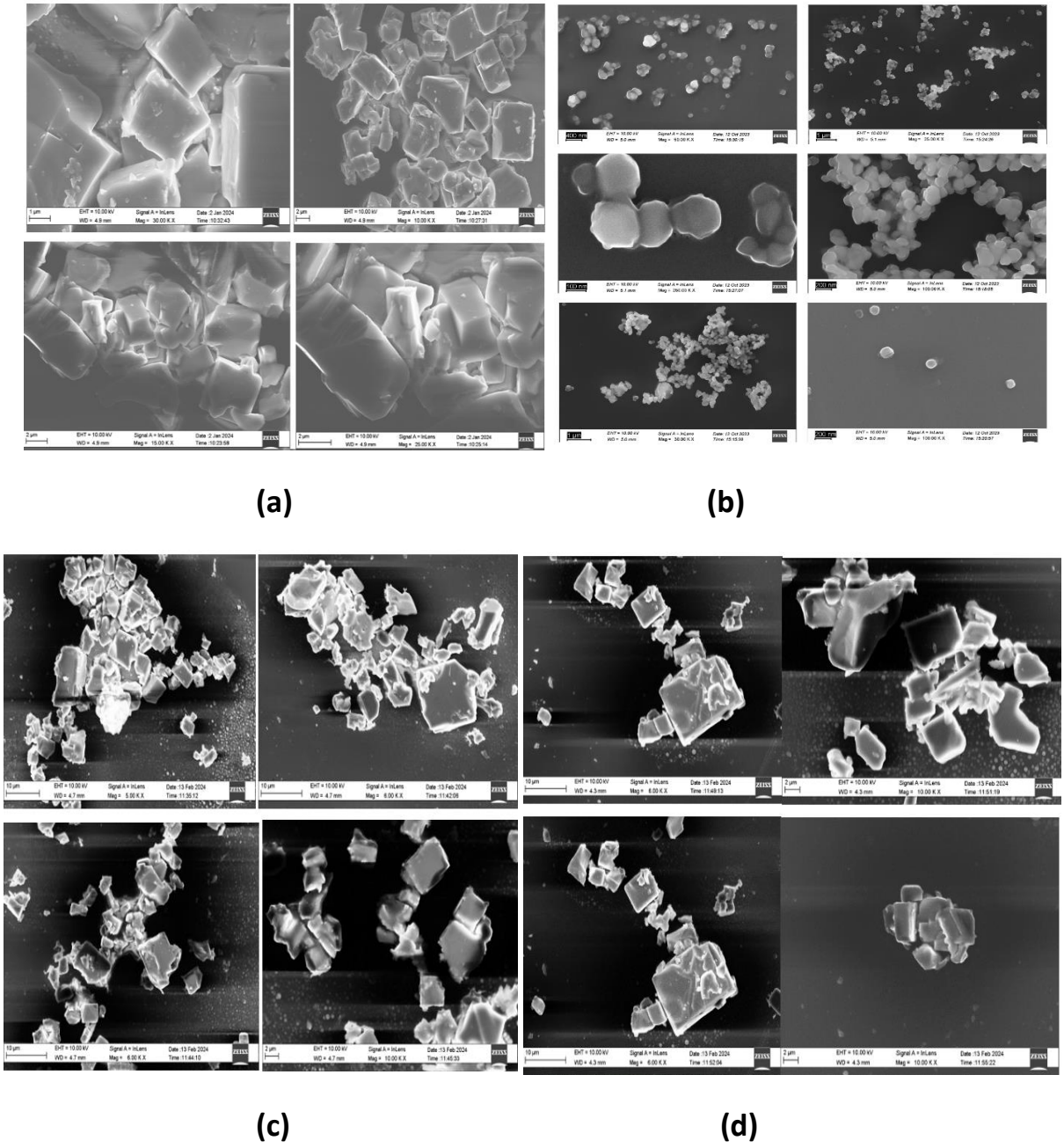


Figure 16: FESEM images of (a)Pure LATP (b)LATP+5%wt PEG (c) LATP+10%wt PEG (d) LATP+15%wt PEG calcined at 900^{o}C

FESEM of model SU70, HITACHI is used for the analysis of the morphology and grain boundary of the sample. From, the above images the morphology and the size of the particles of LATP can be confirmed that a cubicle shape has been formed which is already reported in the literature. So, now we can compare the

morphology of the pure LATP with our PEG% (wt/wt) sample that has been mixed during the 2nd calcination step and ball milled for 24hours.

It has been observed that with the increase in PEG-200 concentration in the LATP calcined sample at 500°C, the morphology of the sample begins to change. It can be seen that initially the morphology was brick like whereas at LATP-25 it was most blunt at the edges.

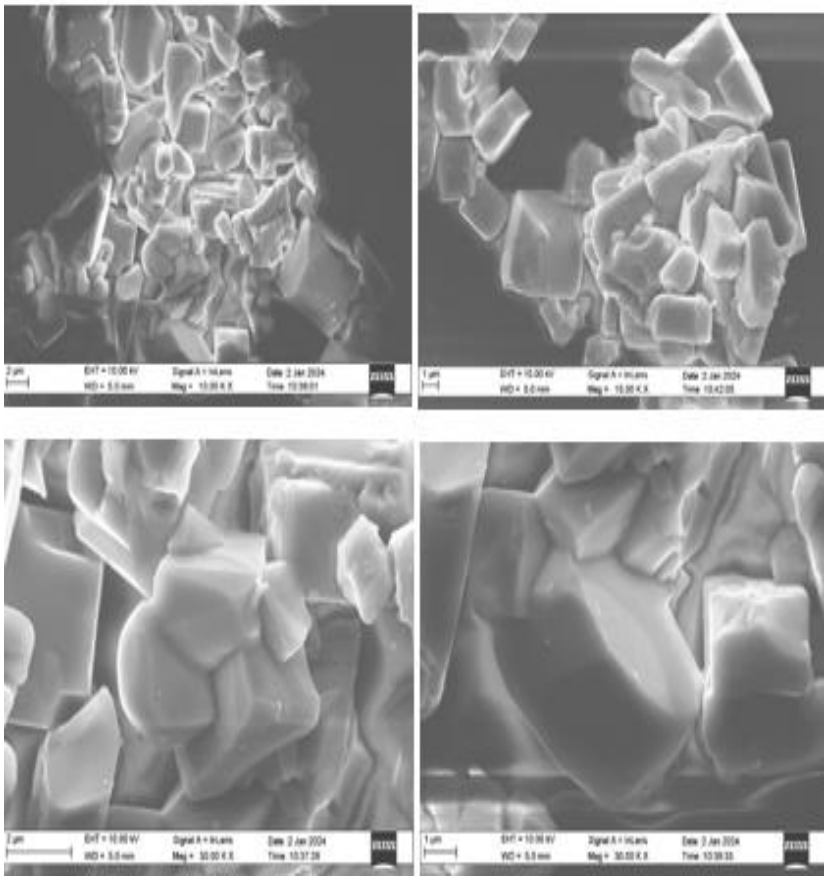
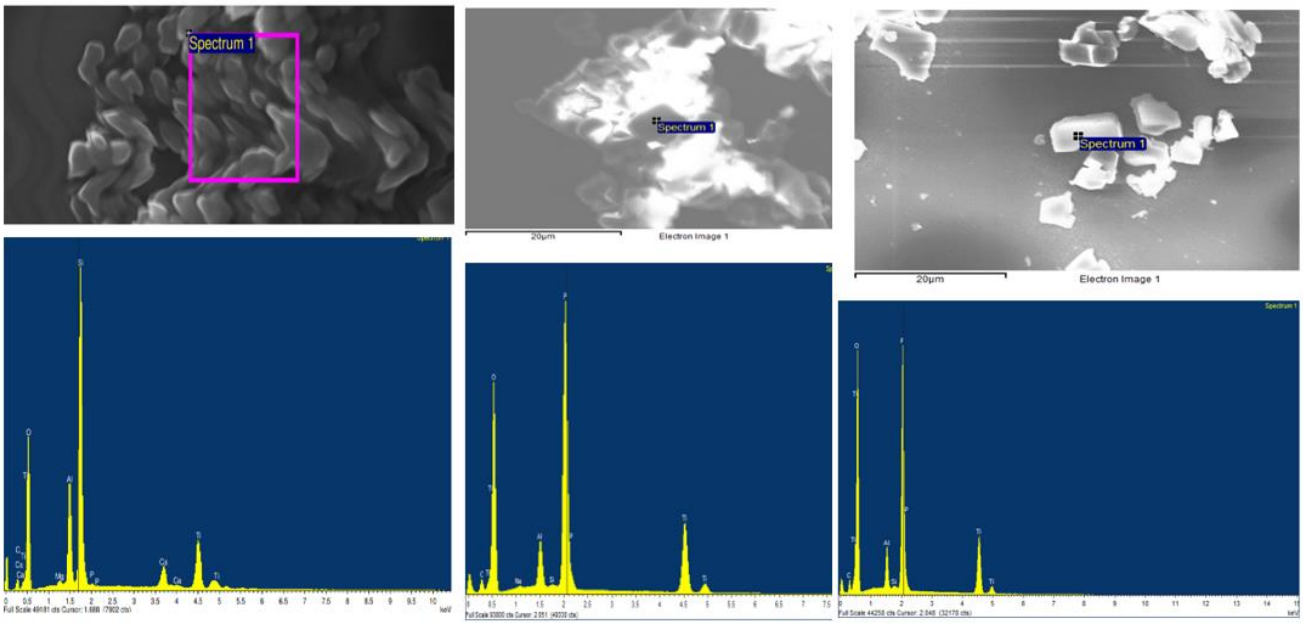


Figure 17: FESEM images of LATP and 25%wt PEG calcined at 900°C

This microstructure engineering can enhance electrochemical properties in our future studies. Increasing the PEG percentage can improve both conductivity and density up to a certain weight percentage. Comparative studies have been conducted further. This morphology has resulted in a reduced agglomerate size and gradually improved ionic conductivity with the increase in PEG% in LATP.

The addition of PEG to LATP does not affect its properties, as it evaporates before the formation of the pure LATP phase.



(a) **(b)** **(c)**

Figure 18: EDX of (a)LATP+5%PEG (b) LATP+10%PEG (c) LATP+15%PEG calcined at 900°C

EDX analysis have been done for the sample mentioned above for various concentration of PEG in LATP to check the elements present in the LATP powder after calcination at 900°C. There are elements apart from Li, Ti, O, P, Al that might get incorporated in the sample from the alumina crucible or the IPA used.

➢ 3.2.3 Fourier Transform Infrared Spectroscopy (FTIR)

The FTIR spectrum was carried out using a JASCO FTIR-6300 spectrometer from a wavenumber of 500 to 4000 cm^{-1}. From the below spectrum we can confirm the chemical composition and molecular structure of our sample. The fingerprint regions in the graphs will decide the functional group present in our material. As, per the literature the main peaks of LATP are observed at 584cm^{-1},642cm^{-1} and 970 cm^{-1}. The band at 584 and 642 cm^{-1} can be attributed to

vibration of TiO^{6-} octahedron whereas the high intensity peak at 937 to 990 cm^{-1} corresponds to the symmetric stretching vibrations of PO_4^{3-} ion.

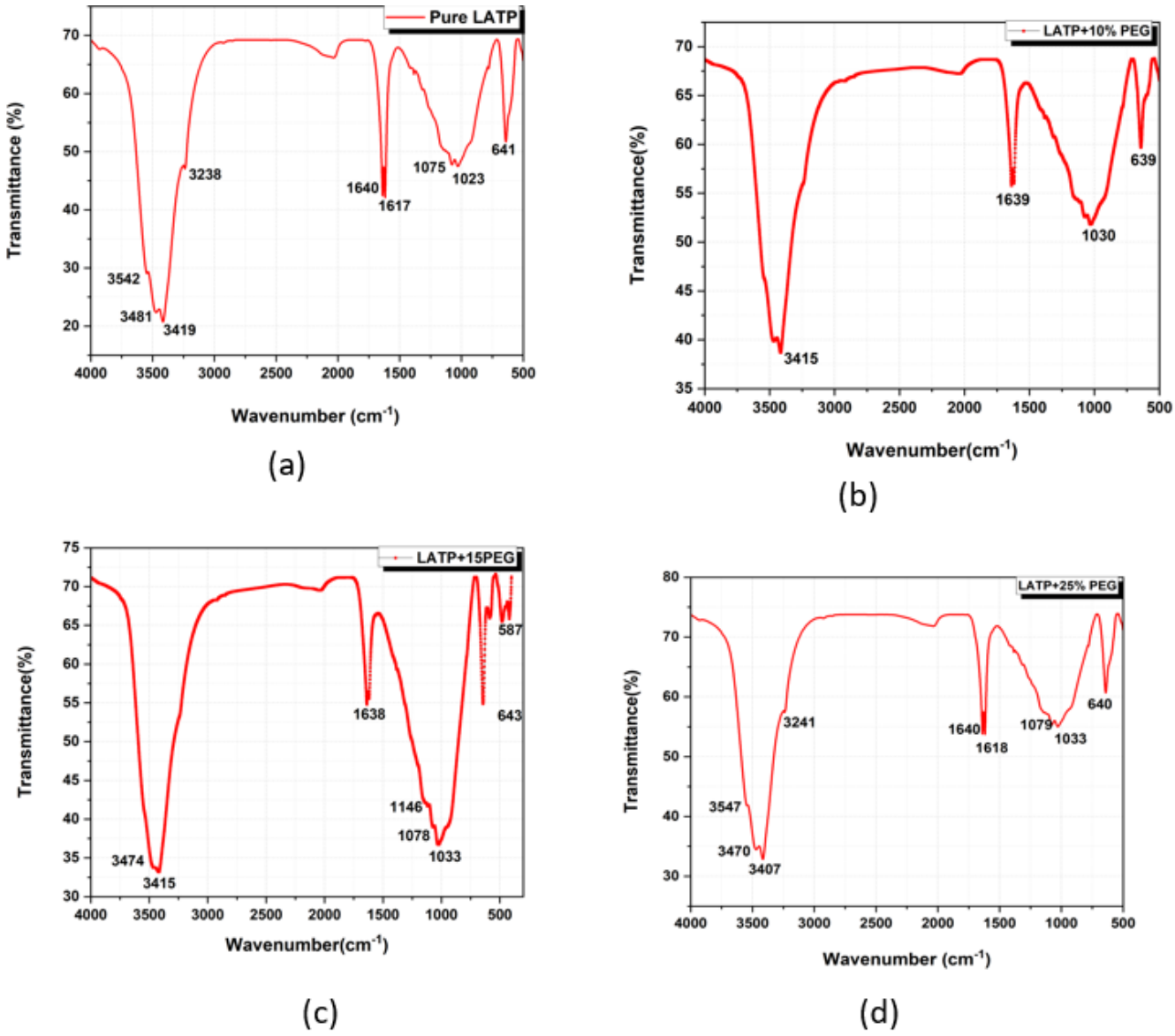


Figure 19: FTIR of (a)Pure LATP (b)LATP+10%PEG (c) LATP+15%PEG (d) LATP+25%PEG calcined at 900°C

➢ 3.2.4 Dynammic Light Scattering (DLS)

The particle size analysis shows that the average particle size of the LATP sample varies with different PEG% content. Sample with different concentration of PEG was dispersed using Isopropyl Alcohol and ultrasonicated for 15mins so that the particles can be well dispersed in the test tube.

Relatively less agglomeration is also seen with 25% PEG in LATP. This comparative particle size study is crucial as it influences conductivity and activation energy studies. Symmetric cell performance will help identify the best among the four PEG variations. Given the difficulty of proceeding with all PEG variations, we will select one variation based on this data.

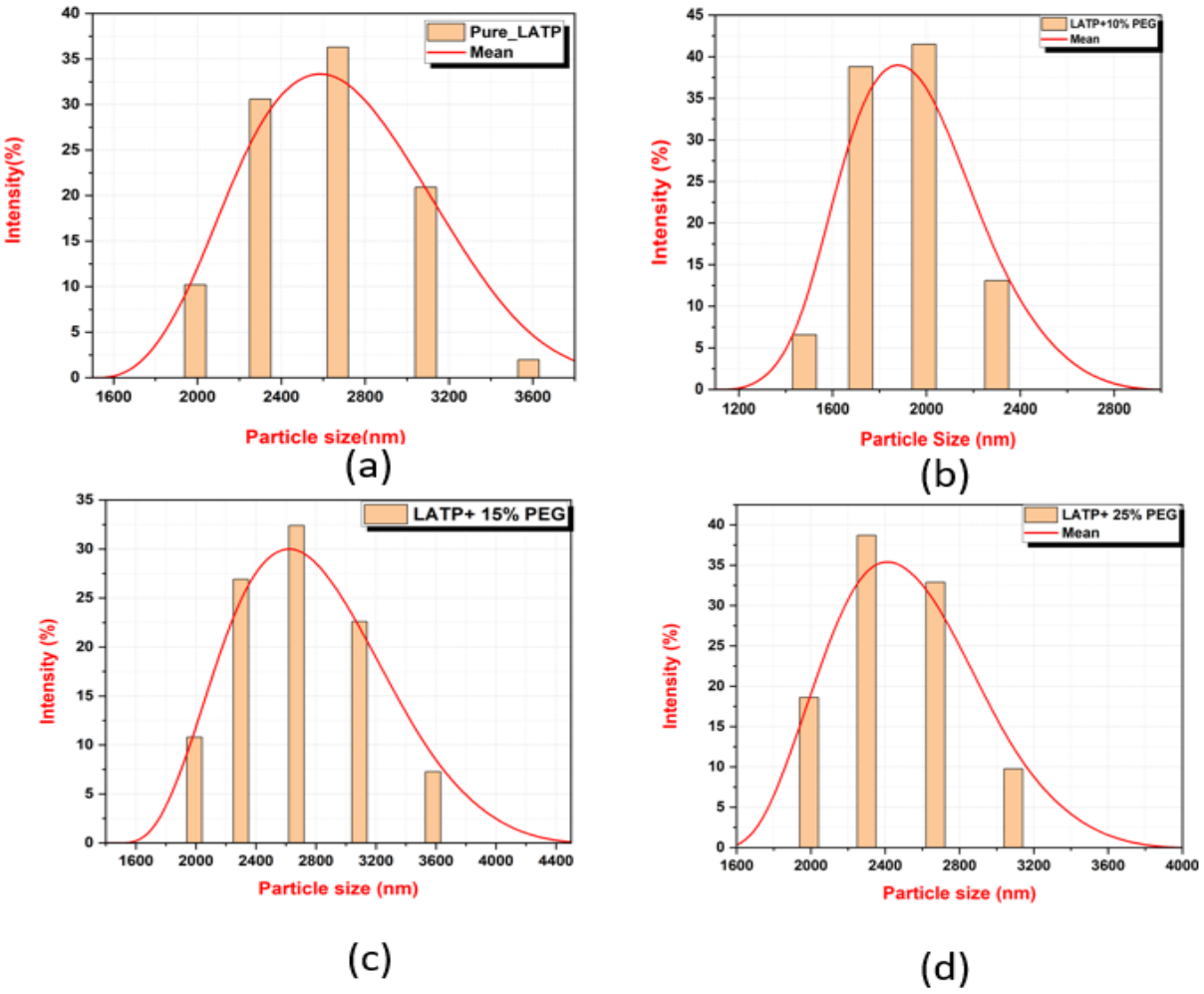


Figure 20: DLS of (a)Pure LATP (b)LATP+10%PEG (c) LATP+15%PEG (d) LATP+25%PEG calcined at 900°C

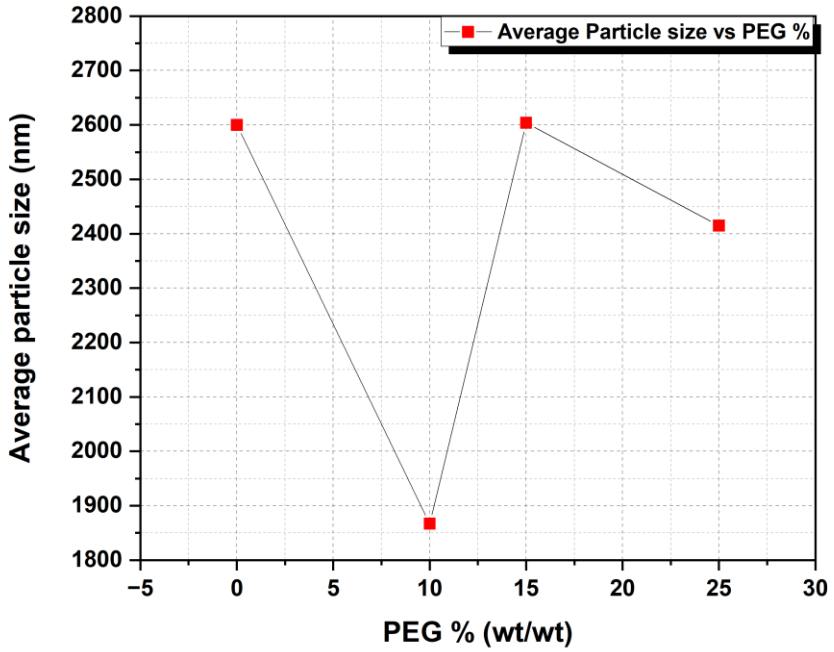


Figure 21: Graphical comparison of average particle size for pristine and PEG variation in LATP.

The variation is plotted against the PEG% in LATP. Increased agglomeration, resulting in larger particle size, is observed with 15% PEG. Low agglomeration is noted with 10% PEG, which significantly reduces particle size compared to other concentrations

➢ 3.3 Thermogravimetry Differential Thermal Analysis (TG-DTA)

In essence, the TG aspect of TG/DTA resembles standard thermogravimetric analysis (TGA), monitoring weight changes relative to temperature under controlled conditions. By plotting the percentage of weight change against the programmed temperature range, researchers can investigate the processes leading to weight fluctuations.

The "DTA" component, short for differential thermal analysis, gauges the temperature discrepancy between the sample and a reference material. This technique reveals peaks or shifts in temperature, denoting specific thermal events occurring within the substance. However, TG/DTA lacks the ability to precisely quantify the heat absorbed or released during these transitions, a parameter known as change in enthalpy (delta H), which is more accurately measured using differential scanning calorimetry (DSC)

The thermogravimetric measurements were carried out using a thermal analyzer (NETZSCH,Germany) under air atmosphere with a constant heating rate of 10°C/min from RT-1200°C. Here in the TGA (thermogravimetric analysis) shows a decrease in initial mass of 2.5% which is due to the loss of moisture and bulk water. Then, a sharp reduction in volume can be observed which is nearly 20% of the mass that is a result of carbonization of organic compound and impurities which is not needed for the pure phase LATP formation.

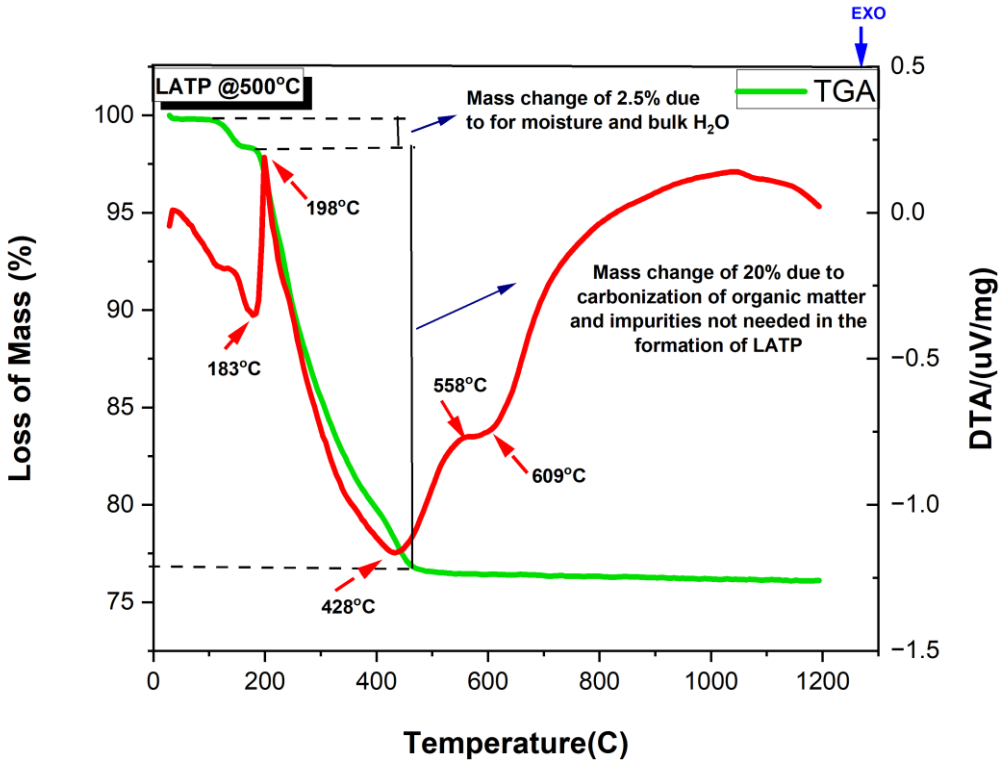


Figure 22: TG-DTA for ash synthesized LATP powder dried after ball milling for 24hours done at temperature (0-1200°C).

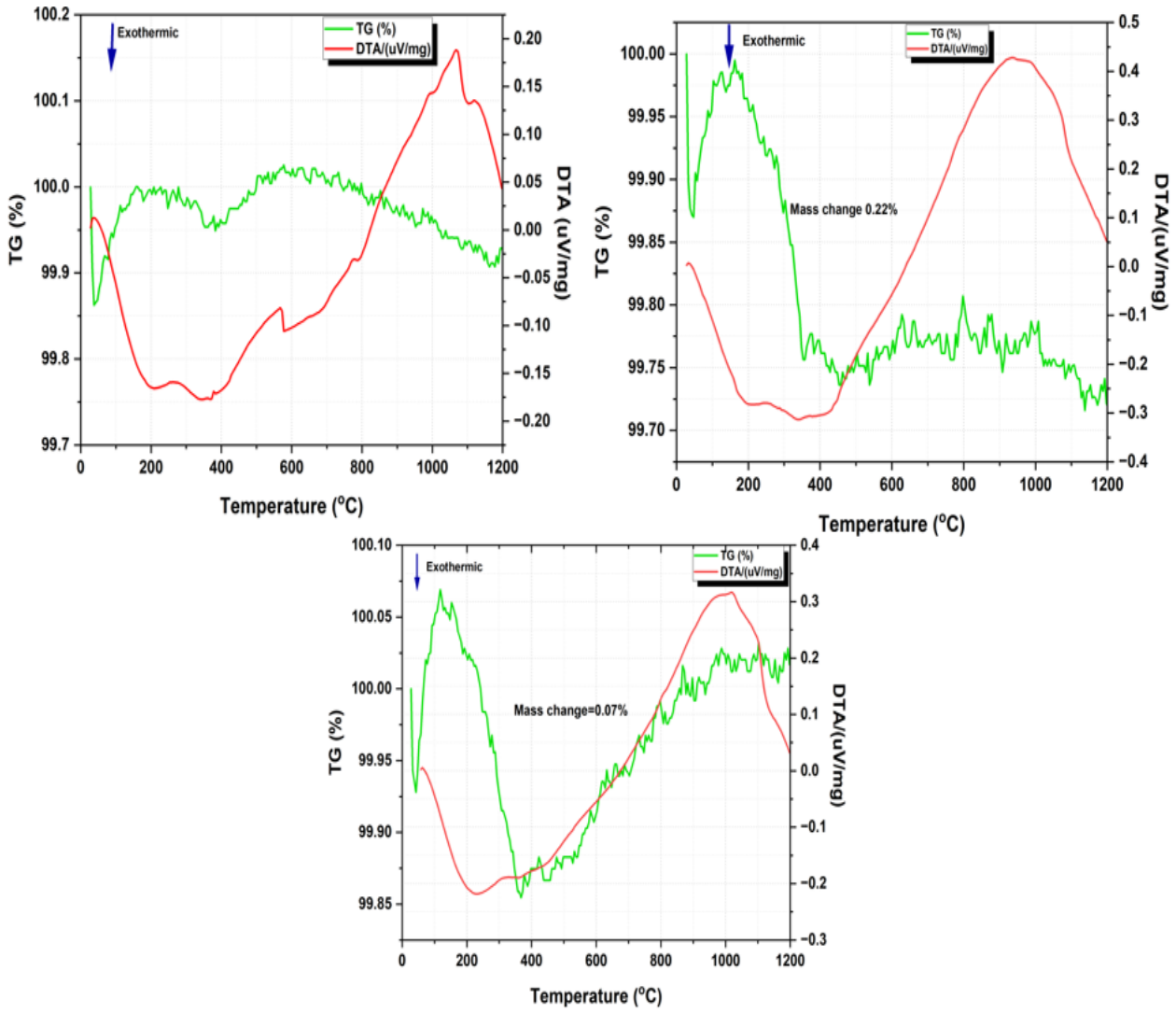


Figure 23: TG-DTA for (a) LATP+10% PEG (b) LATP+15% PEG (c) LATP+25% PEG

From the TG-DTA graph above, we can conclude that the mass change is negligible for the sample where PEG-200 has already been added to the LATP powder. As the PEG-200 content increases, the mass change becomes more pronounced compared to LATP-10. This increase is due to the evaporation of PEG-200, a polymer, from the LATP sample once it exceeds the melting point of PEG-200. The higher the wt% of PEG-200, the greater the weight loss and mass change.

3.4 Density calculation using Archimedes principle

❖ Green Density calculation

The data was taken before the experimental study in Toluene which is used as liquid medium for the density calculation. Based on the liquid which has to be chemically unreactive with the specimen sample that is used for density calculation. As per the theoretical value the density of pure LATP is 2.92 g/cc.

Table 5: Green density calculation

SI No.	PEG% (wt/wt)	Thickness (cm)	Diameter (cm)	Weight (g)	Density g/cc)
1	0	0.17	0.97	0.3239	2.5772
2.	5	0.18	0.98	0.4841	1.9931
3	10	0.182	0.98	0.3657	1.9931
4	15	0.16	0.98	0.3070	2.5427
5	25	0.18	0.97	0.3299	2.4067

➢ Archimedes Density

The samples were dipped in Toluene for 10hours inside a vacuum desicator to prevent the contact with the atmosphere. The setup was undisturbed and archimedes measurement unit was used for the weight measurement both in air and inside the liquid medium. The density of the liquid medium is already known to us.

$$\frac{\text{Density of the sample}}{\text{Density of Toluene}} = \frac{\text{Weight of the sample in air}}{\text{Weight of the sample in air} - \text{Weight of the sample in Toluene}}$$

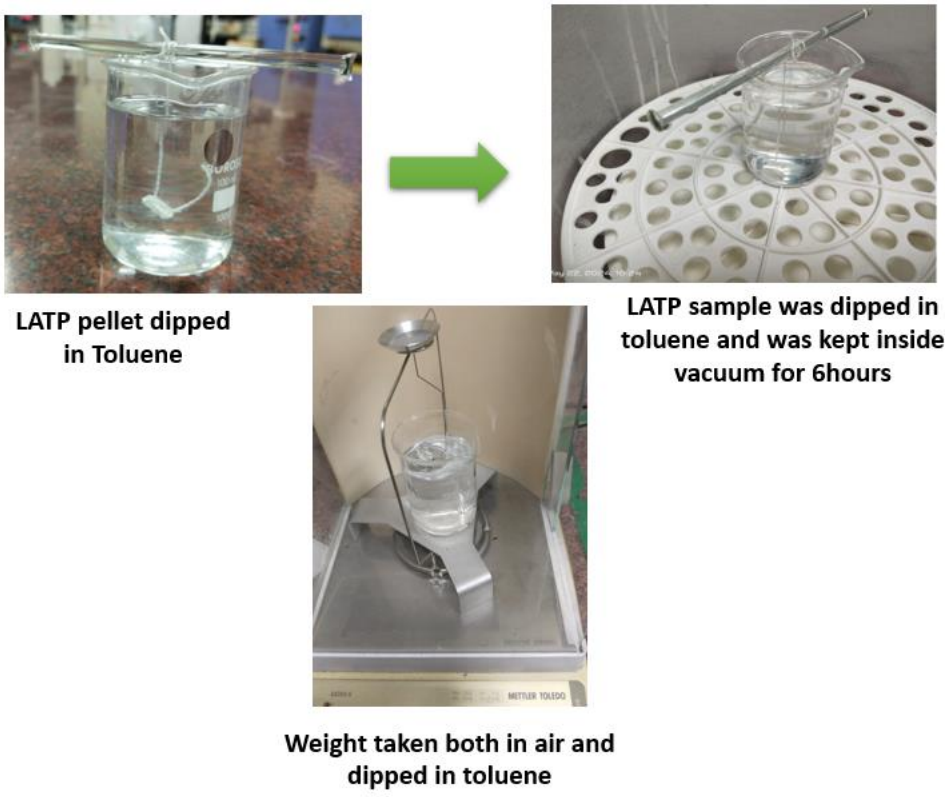


Figure 24: Experimental procedure to measure the density of LATP using Archimedes method.

SI No.	PEG% (wt/wt)	Weight in air (g)	Weight in Toluene (g)	Density (g/cc)	Percentage of theoretical density (%)
1	0	0.17	0.97	2.5772	93.01
2.	5	0.18	0.98	1.9931	81.8
3	10	0.182	0.98	1.9931	94.07
4	15	0.16	0.98	2.5427	93.77
5	25	0.18	0.97	2.4067	94.28

Table 6: Density calculation using Archimedes principle

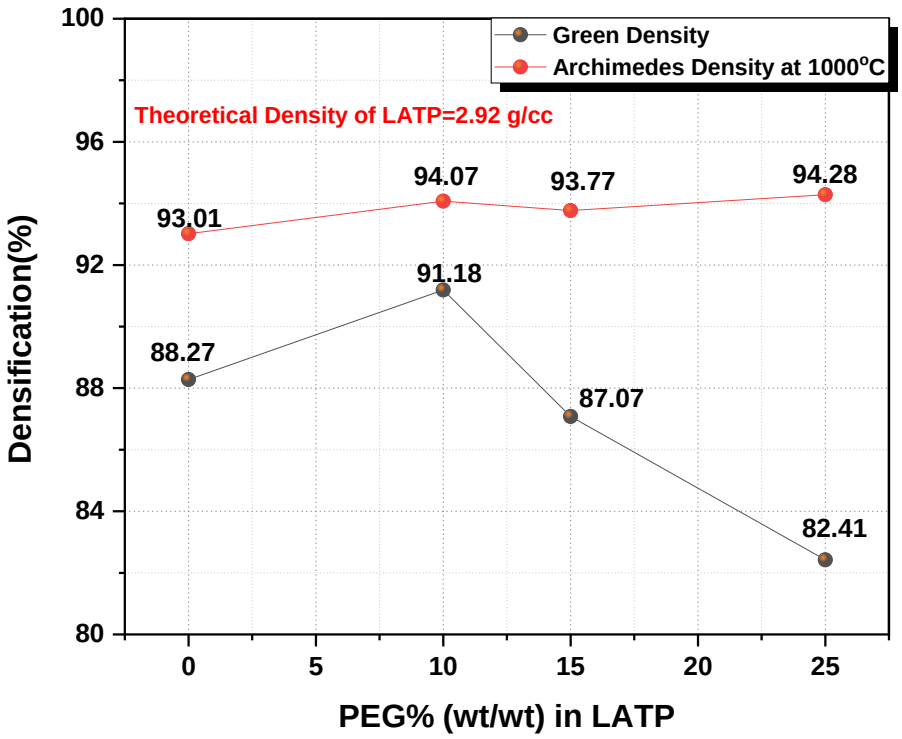
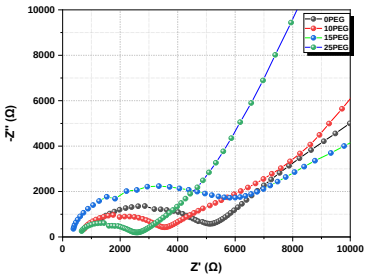


Figure 25: The relation between density calculated by Archimedes principle and the green density calculated

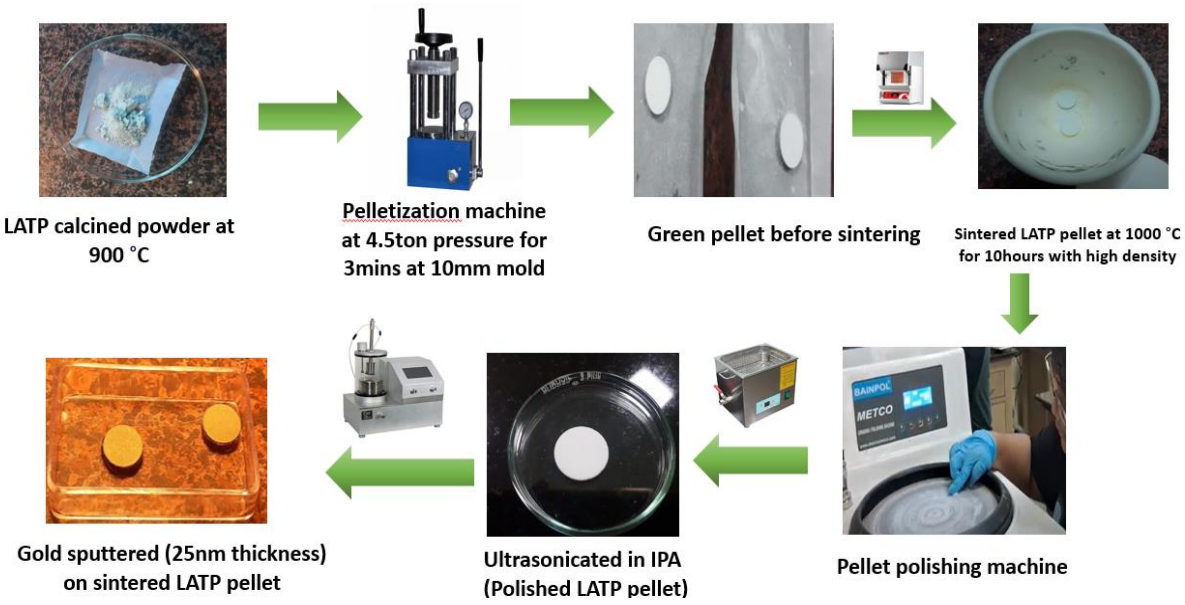
The density calculation can be observed for pristine and varied PEG % (wt/wt) in LATP. The theoretical study has been marked in black whereas the Archimedes study is marked in red to make a distinguish comparison. The theoretical density for LATP has been reported to be 2.9g/cc. The density of the LATP-10 is seen to be the maximum among all. As, we can see the green density study has not been that accurate as compare to the Archimedes calculation. The gap or the jump that can be observed incase of Archimedes studies is much more than green density calculation. Thus, we can say that LATP has highest density value comparing to other NASICON type Solid state electrolyte like LLZO which has density of nearly 70% to its theoretical value. High density has advantage like ensures closer packing of ions and minimizes the occurrence of defects, such as voids or pores, within the material. This allows for better ion transport pathways and thus improves the overall ionic conductivity of the SSE.

CHAPTER-4



Electrochemical studies of LATP: $Li_{1.5}Al_{0.5}Ti_{1.5}(PO_4)_3$

- ❖ Ionic transport properties
- ❖ Symmetric cell and Plating/striping behavior
- ❖ Electrochemical cell performance studies



Electrochemical studies of LATP as solid-state electrolyte

Chapter 4

"This chapter traces the study of LATP solid state electrolyte. Starting from its synthesis from precursor, characterization of the powder and its electrochemical studies. Symmetric cell study of the symmetric cell has been done along Lithium foil on both sides."

4.1 Ionic conductivity and transport properties

Li-ion transport mechanisms in solid-state ceramic electrolytes primarily include the vacancy mechanism, interstitial mechanism, and interstitial–substitutional exchange mechanism. The vacancy mechanism relies on Schottky defects, which create numerous vacancies for ion hopping through the crystal. When a Li^+ ion hops, a new vacancy is created in its original position, enabling continuous Li+ ion transport through this cycle. In the interstitial mechanism, interstitial ions diffuse through Frenkel defects, with interstitial Li^+ ions moving between molecular skeletons by displacing Li ions in adjacent available sites. For any given ceramic solid electrolyte, the Li-ion transport mechanism depends on three factors: carrier type, diffusion pathway, and diffusion type. Carrier types and concentrations are determined by point defects in the ceramic crystal structures, directly affecting ionic conductivity. Li^+ ions interact with each other and their surroundings during transport, significantly influencing ionic conductivity.

- **Sample preparation for the electrochemical studies**

  A pellet was prepared using the LATP sample calcined at 900°C. For each pellet, 0.5g of the sample was used, along with 1 wt% of PVDF binder. The PVDF was ground in IPA to ensure thorough mixing. The mixture was ground in a mortar and pestle until the IPA evaporated and a solid powder formed. This solid powder was then thoroughly mixed in the mortar and pestle. The resulting mixture was placed in a pellet machine and subjected to 4.5 tons of pressure for 3 minutes to form the pellet.

The sintering of the pellets was done at 1000°C for 10 hours at 120°C/min in a Carbolite furnace to reduce the grain boundary as a result which will result in the reduction of grain boundary resistance. This also helps to increase the density of the pellets by decreasing the porosity which resulted in nearly to 94% of the theoretical value calculated. This also results in increase of mechanical strength of the ceramic material due to the significant reduction in the gaps between each particle.

Gold sputtering is done to get a conducting surface over the LATP. The sintered pellet was gold coated for 55sec with a thickness of 20-25nm. After each side coating a 10mins drying time is considered before next sputtering. Before the sputtering is performed masking of the edges of the surface is to be done so that the coating is not spread out or on the edges which might result in the short circuit. The gold coating in this case can be replaced with either silver or platinum and can be used as a current collector. While deposition we need to make sure of even thickness of the contact material on both sides resulting in a accurate result.

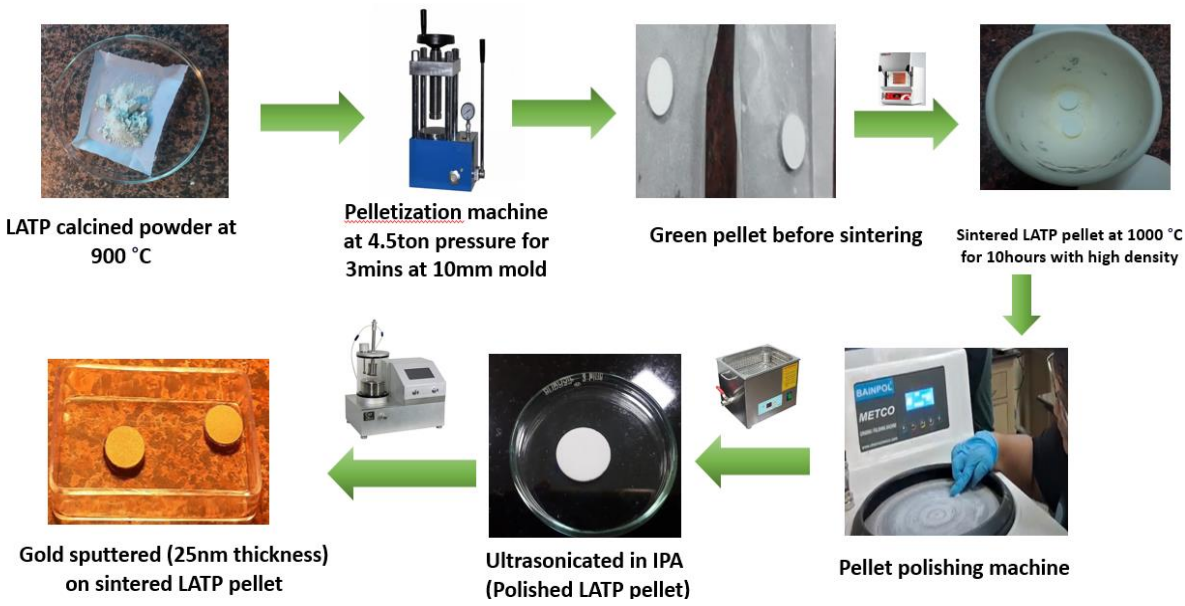


Figure 26: Process of preparing LATP pellet for electrochemical studies

➢ Electrochemical Impedance Spectroscopy calculation at room temperature for Pure LATP & variations of PEG %

Electrochemical impedance spectroscopy (EIS) measurements were used to determine the Li-ion conductivity of pure LATP and composite membranes. These measurements were conducted in the frequency range from 1 MHz to 1 Hz with an amplitude of 300 mV using a ZIVE potentiostat. Additionally, the temperature dependence of the Li-ion conductivity for both pure LATP and other varied PEG percentage was recorded.

Electrochemical Impedance Spectroscopy has been done for all the variation of PEG % in LATP along with pristine LATP to compare the ionic conductivity at room temperature. The average pellet size has a thickness of 1.7mm and a diameter of 10mm. The pellets were gold coated on both the sides to create a contact. When we calculated with the formula as

$$\sigma = L/R*A$$

where L=Thickness of the pellet
A=Area of the pellet with diameter
R=Resistance

After the electrochemical impedance spectroscopy based on the suitable result further charge discharge profile has been checked using battery cycler. Both the activation energy and ionic conductivity at room temperature and at a temperature range of (30-120) ^{o}C has been checked for the all PEG variation in LATP. To check the electrode and interface stability of the solid-state electrolyte further lithium foil has been used in the symmetric cell testing.

❖ Electrochemical Impedance Spectroscopy data for Pure LATP

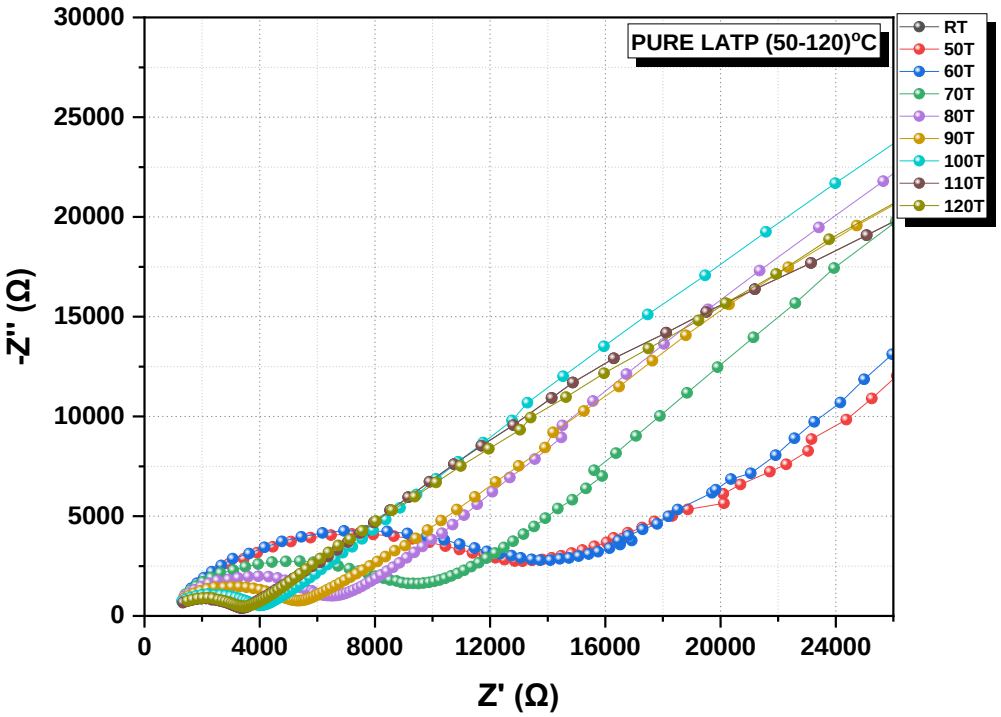


Figure 27: EIS data of pure LATP at variation of temperature from RT-120°C

The diameter of the pellet for which the EIS was done was 1.5mm of thickness with a diameter of 9.7mm. The pellet was sintered at 1000°C for 10hours and then gold coating was deposited on the pellet using sputtering technique. As, we can see that with gradual increase in the temperature the conductivity value is decreasing. Later, from the above data we have also calculated the activation energy of the samples.

The Nyquist plot for the pure LATP given above shows that there is gradual decrease in ionic conductivity from (50-120) ° C. The activation energy for the pure LATP has been found to be 0.44eV where the calculation

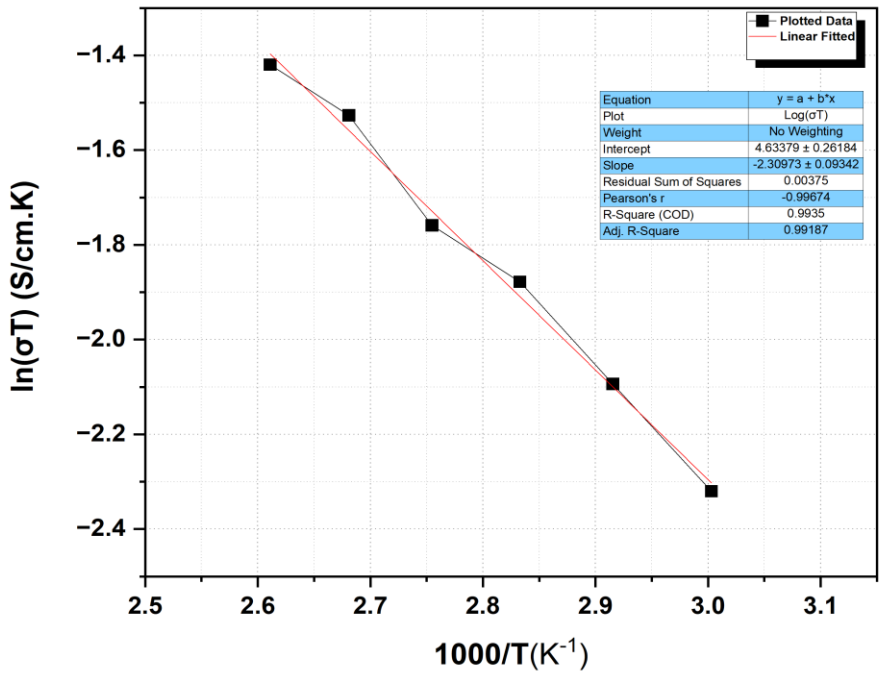


Figure 28: Activation energy plotted from (RT-120) °C for pristine LATP

Dia(mm)	Radius(cm)	Thick(cm)/	Area	Temperature	Bulk R	GB R	Bulk Cond
9.7	0.485	0.15	0.738981	50	13964	0	1.45361E-05
9.7	0.485	0.15	0.738981	60	14123	0	1.43725E-05
9.7	0.485	0.15	0.738981	70	8635	0	2.35069E-05
9.7	0.485	0.15	0.738981	80	5410	0	3.75198E-05
9.7	0.485	0.15	0.738981	90	4228	0	4.80091E-05
9.7	0.485	0.15	0.738981	100	2545	0	7.97573E-05
9.7	0.485	0.15	0.738981	110	2042	0	9.94037E-05
9.7	0.485	0.15	0.738981	120	1993	0	0.000101848

Table 7: Data for Conductivity calculation at a temperature of (RT-120) ° C

Temp	Temp in K	1000/T	Log(σT)Bulk	Log(σT)GB	Log(σT)Total	Slope	Activation Energy
50	323	3.095975232	-2.328349042	#NUM!	#NUM!		
60	333	3.003003003	-2.32002445				
70	343	2.915451895	-2.093509946			-2.23	0.442542407
80	353	2.83286119	-1.877964284				
90	363	2.754820937	-1.758770078				
100	373	2.680965147	-1.526520679				
110	383	2.610966057	-1.419398688				
120	393	2.544529262	-1.397656472				

Table 8: Data for Activation energy calculation at a temperature of (RT-120) ° C

❖ Electrochemical Impedance Spectroscopy data for LATP-5

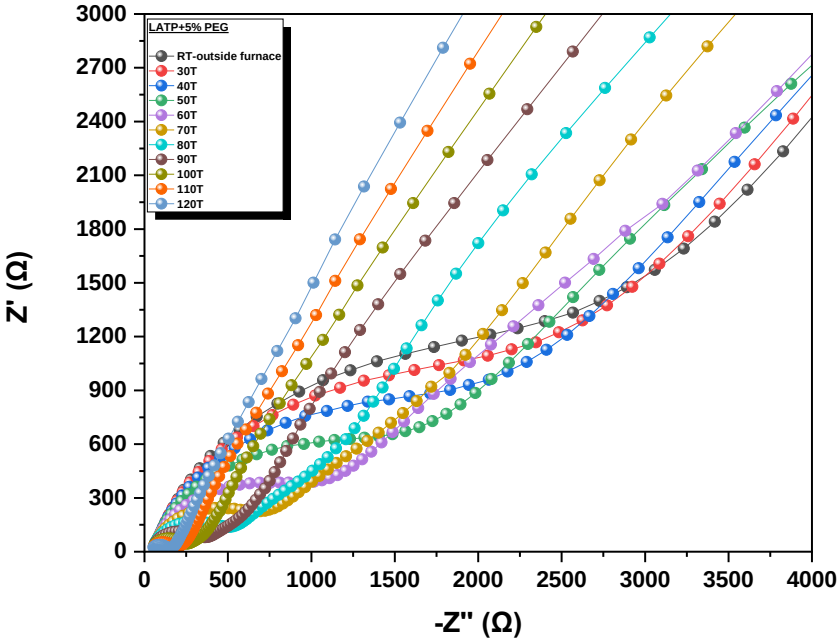


Figure 29: EIS data of LATP-5 at variation of temperature from RT-120^{o}C

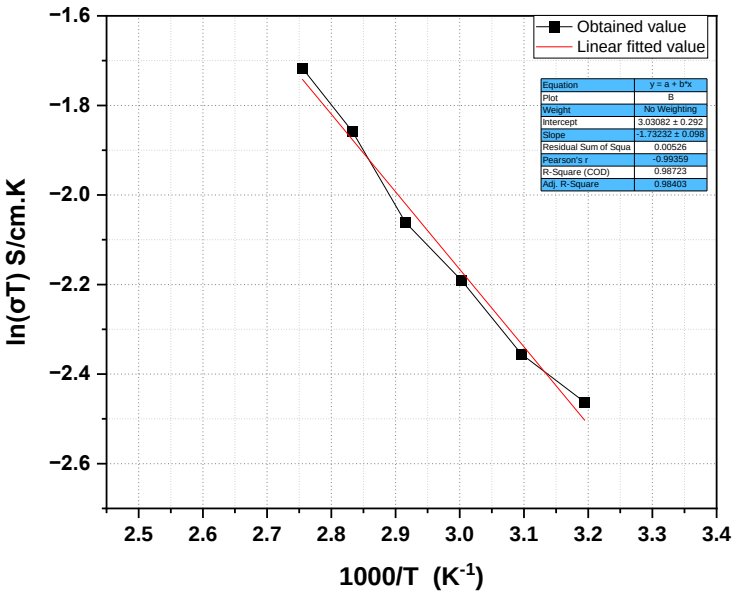


Figure 30: Activation energy plotted from (RT-120) ^{o}C for LATP-5

Dia(mm)	Radius(cm)	Thick(cm)/	Area	Temperature		Bulk R	GB R	Bulk Cond
18.9	0.945	0.09	2.80552	30		3413	0	9.39925E-06
18.9	0.945	0.09	2.80552	40		2916	0	1.10012E-05
18.9	0.945	0.09	2.80552	50		2347	0	1.36684E-05
18.9	0.945	0.09	2.80552	60		1659	0	1.93367E-05
18.9	0.945	0.09	2.80552	70		1267	0	2.53194E-05
18.9	0.945	0.09	2.80552	80		817	0	3.92652E-05
18.9	0.945	0.09	2.80552	90		606	0	5.29367E-05
18.9	0.945	0.09	2.80552	100		329	0	9.75065E-05
18.9	0.945	0.09	2.80552	110		165	0	0.000194422
18.9	0.945	0.09	2.80552	120		143	0	0.000224333

Table 9: Data for Conductivity calculation at a temperature of (RT-120) °C

Temp	Temp in K	1000/T	Log(σT)Bulk	Log(σT)GB	Log(σT)Total	Slope	Activation Energy
30	303	3.300330033	-2.545464273	#NUM!	#NUM!		
40	313	3.194888179	-2.463013796				
50	323	3.095975232	-2.355081181				
60	333	3.003003003	-2.191172766				
70	343	2.915451895	-2.061253108			-1.73	0.343317652
80	353	2.83286119	-1.858217965				
90	363	2.754820937	-1.716336613				
100	373	2.680965147	-1.43925768				
110	383	2.610966057	-1.128055784				
120	393	2.544529262	-1.054714101				

Table 10: Data for Activation energy calculation at a temperature of (RT-120) °C

❖ Electrochemical Impedance Spectroscopy data for LATP-10

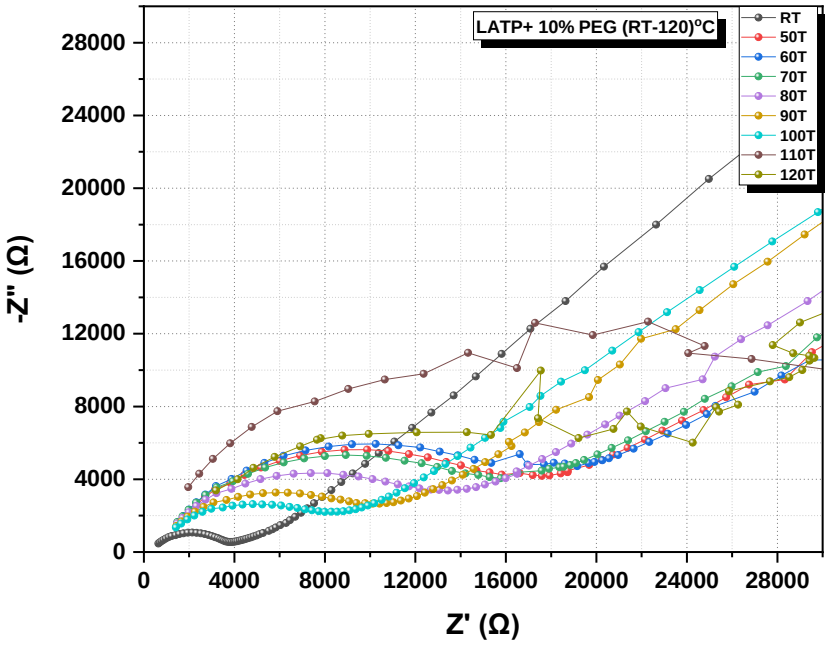


Figure 31: EIS data of LATP-10 at variation of temperature from RT-120°C

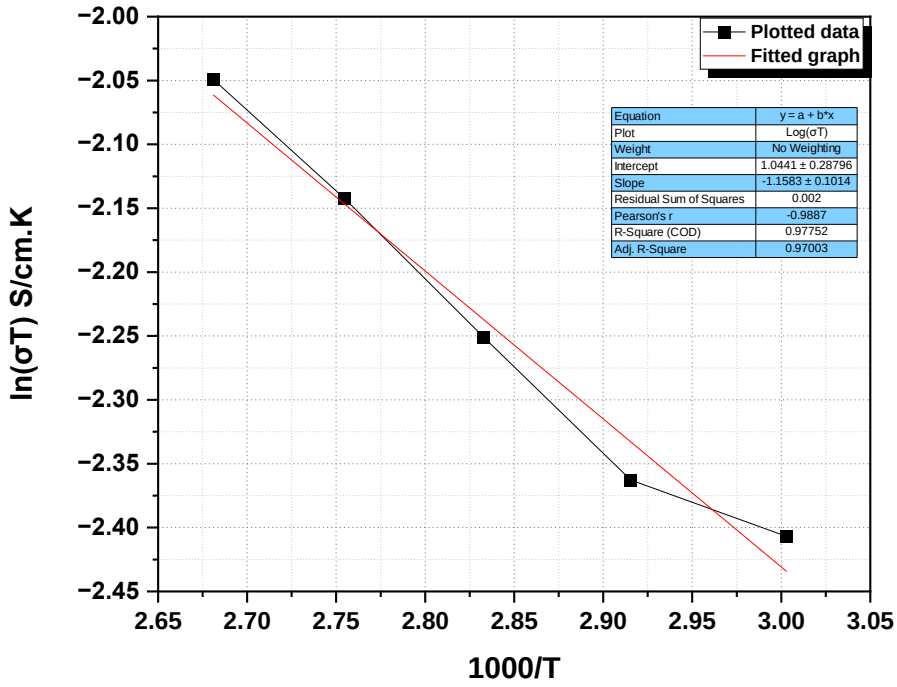


Figure 32: Activation energy plotted from (RT-120) °C for LATP-10

Dia(mm)	Radius(cm)	Thick(cm)	Area	Temperature	Bulk R	GB R	Bulk Cond	GB Conduc	Total R	Total Conduc
9.68	0.484	0.14	0.73594	50	15637	0	1.21656E-05			
9.68	0.484	0.14	0.73594	60	16169	0	1.17653E-05	#DIV/0!	16169	1.17653E-05
9.68	0.484	0.14	0.73594	70	15045	0	1.26443E-05			
9.68	0.484	0.14	0.73594	80	11970	0	1.58926E-05			
9.68	0.484	0.14	0.73594	90	9587	0	1.98429E-05			
9.68	0.484	0.14	0.73594	100	7946	0	2.39408E-05			

Table 11: Data for Conductivity calculation at a temperature of (RT-120) ° C

Temp	Temp in K	1000/T	Log(σT)Bulk	Log(σT)GB	Log(σT)Total	Slope	Activation Energy
50	323	3.095975232	-2.405663107	#DIV/0!	-2.45517909		
60	333	3.003003003	-2.406951121				
70	343	2.915451895	-2.362810266			-1.15	0.228216937
80	353	2.83286119	-2.251031638				
90	363	2.754820937	-2.142488296				
100	373	2.680965147	-2.049151922				

Table 12: Data for Activation energy calculation at a temperature of (RT-120) ° C

❖ Electrochemical Impedance Spectroscopy data for LATP-15

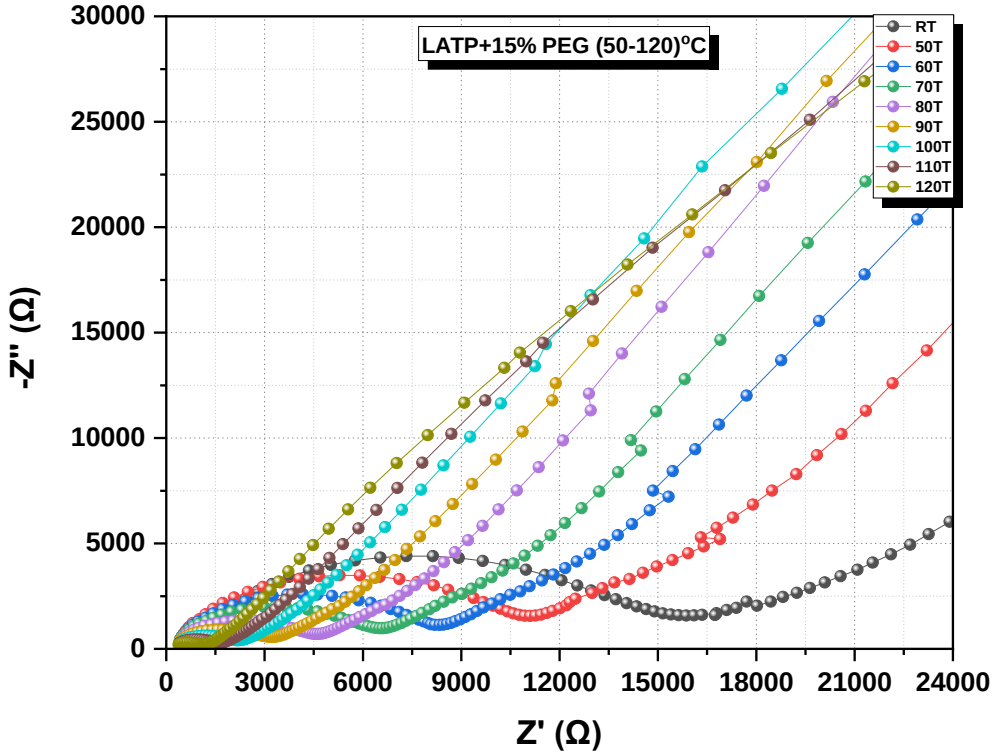


Figure 33: EIS data of LATP-15 at variation of temperature from RT-120°C

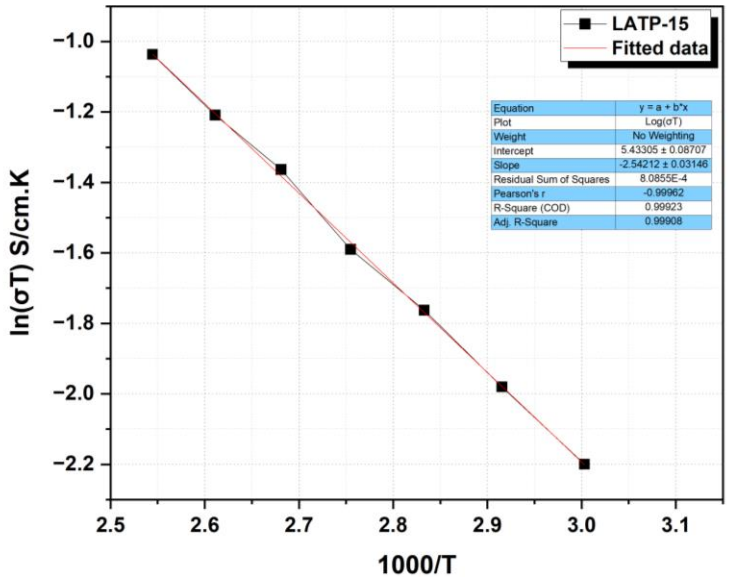


Figure 34: Activation energy plotted from (RT-120)°C for LATP-15

Dia(mm)	Radius(cm)	Thick(cm)	Area	Temperature		Bulk R	GB R	Bulk Cond
9.72	0.486	0.15	0.74203	50		10495	0	1.92614E-05
9.72	0.486	0.15	0.74203	60		10656	0	1.89703E-05
9.72	0.486	0.15	0.74203	70		6622	0	3.05267E-05
9.72	0.486	0.15	0.74203	80		4129	0	4.89581E-05
9.72	0.486	0.15	0.74203	90		2852	0	7.08793E-05
9.72	0.486	0.15	0.74203	100		1740	0	0.000116177
9.72	0.486	0.15	0.74203	110		1252	0	0.00016146
9.72	0.486	0.15	0.74203	120		864	0	0.000233967

Table 13: Data for Conductivity calculation for LATP-15 at a temperature of (RT-120)°C

Temp	Temp in K	1000/T	Log(σT)Bulk	Log(σT)GB	Log(σT)Total	Slope	Activation Energy
50	323	3.095975232	-2.206110706	#DIV/0!	-2.247708733		
60	333	3.003003003	-2.199480764				
70	343	2.915451895	-1.980025842			-2.54	0.504061755
80	353	2.83286119	-1.762400963				
90	363	2.754820937	-1.589573681				
100	373	2.680965147	-1.363171202				
110	383	2.610966057	-1.20873634				
120	393	2.544529262	-1.036451977				

Table 14: Data for Activation energy calculation for LATP-15 at a temperature of (RT-120)°C

❖ Electrochemical Impedance Spectroscopy data for LATP-25

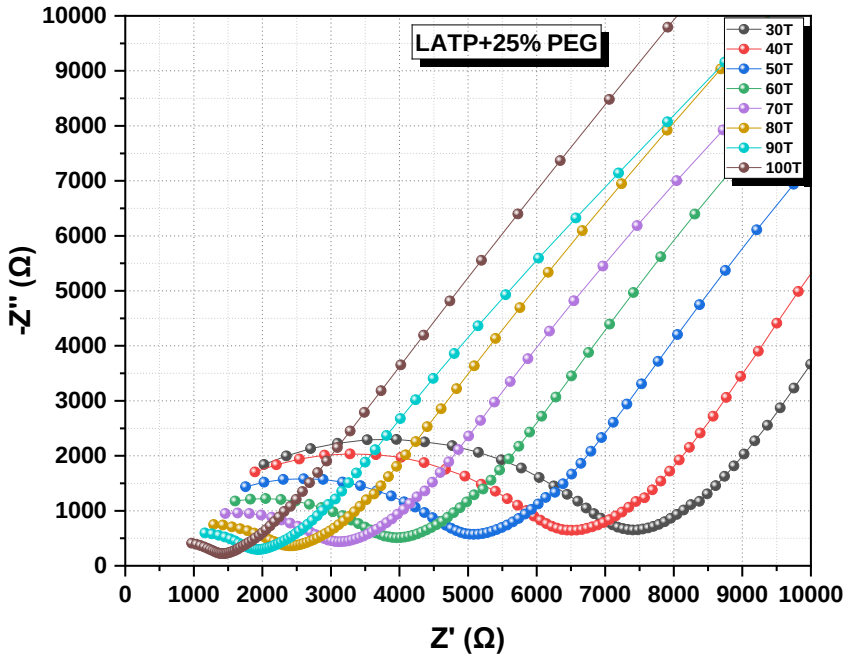


Figure 35: EIS data of LATP-25 at variation of temperature from RT-100°C

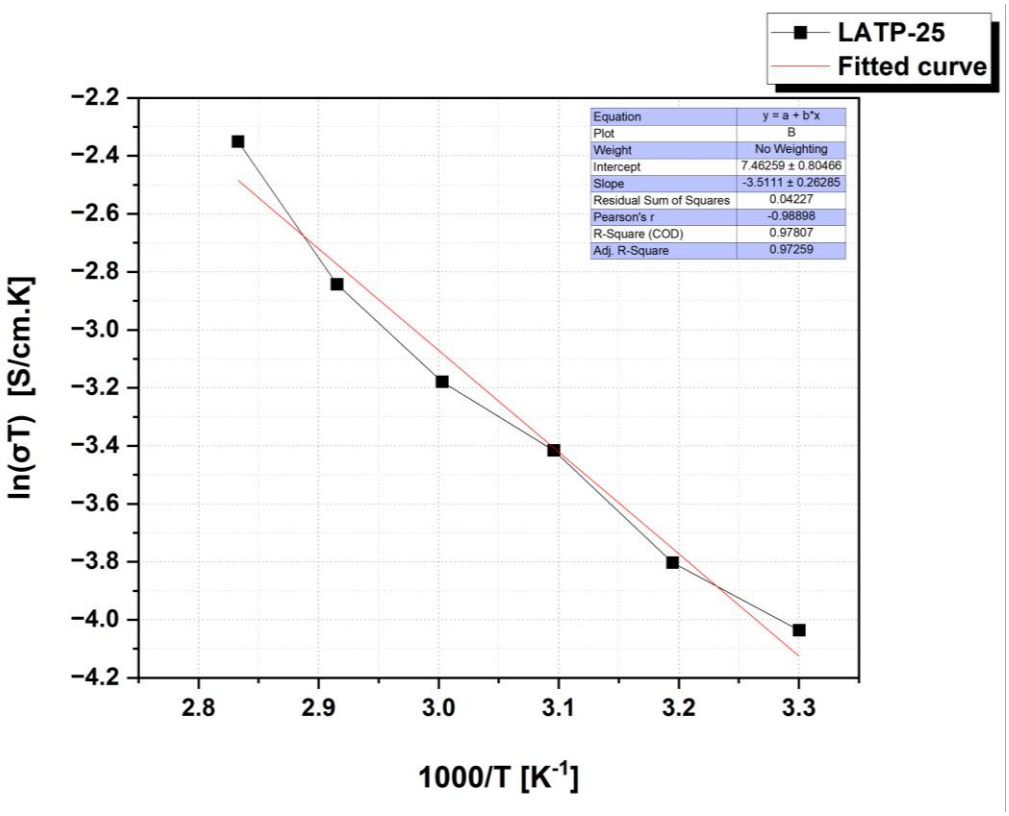


Figure 36: Activation energy plotted from (30-100)°C for LATP-25

Dia(mm)	Radius(cm)	Thick(cm)	Area	Temperature	Bulk R	GB R	Bulk Cond
9.7	0.485	0.234	0.73898	30	5431	0	5.83046E-05
9.7	0.485	0.234	0.73898	40	4442	0	7.1286E-05
9.7	0.485	0.234	0.73898	50	3113	0	0.000101719
9.7	0.485	0.234	0.73898	60	2533	0	0.000125011
9.7	0.485	0.234	0.73898	70	1864	0	0.000169878
9.7	0.485	0.234	0.73898	80	1173	0	0.000269951
9.7	0.485	0.234	0.73898	90	903	0	0.000350667
9.7	0.485	0.234	0.73898	100	562	0	0.000563439

Table 15: Data for Conductivity calculation for LATP-25 at a temperature of (RT-120)°C

Temp	Temp in K	1000/T	Log(σT)Bulk	Log(σT)GB	Log(σT)Total	Slope	Activation Energy
30	303	3.300330033	-4.036096181	#DIV/0!	-1.672779416		
40	313	3.194888179	-3.802607243				
50	323	3.095975232	-3.415640276			-3.198	0.634641533
60	333	3.003003003	-3.178967589				
70	343	2.915451895	-2.842699977				
80	353	2.83286119	-2.35080222				
90	363	2.754820937	-2.061270148				
100	373	2.680965147	-1.559873859				

Table 16: Data for Activation energy calculation for LATP-25 at a temperature of (RT-100)°C

❖ **Comparison among all the ionic conductivity of pure LATP and PEG incorporated LATP for varied percentage**

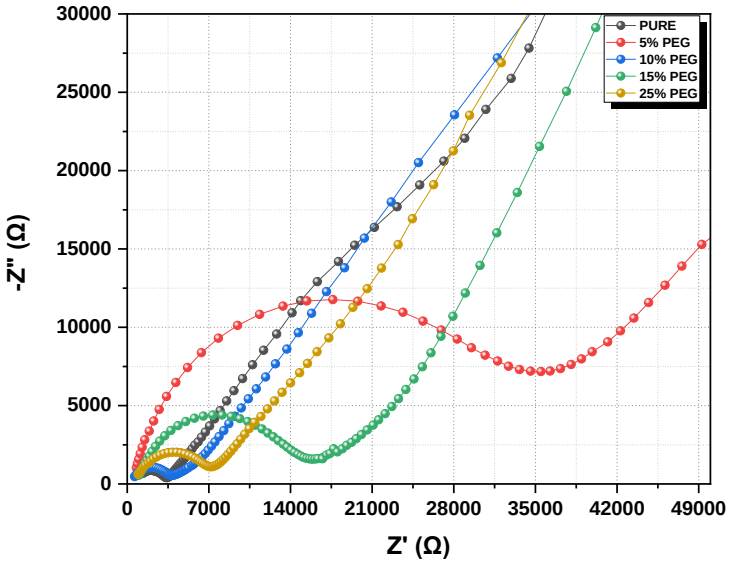


Figure 37: EIS data of pure LATP and PEG% variation at room temperature

We have found that conductivity of the PEG % 25 in LATP is maximum among all with $1.4X10^{-4}$S/cm at room temperature followed by the LATP-10 with $1X10^{-4}$ S/cm. A comparison graph has been given below for the easy understanding of the conductivity at room temperature. The pellet was sintered at 1000°C and gold coating was sputtered on both sides.

The activation energy comparison if done we can see a pattern where the pure LATP from a temperature of (50-120) ° C has a activation energy of 0.44eV a value near to reported data in literature that is 0.39eV. The lowest activation energy was found in case of LATP-10 that is 0.22eV and gradually for the later variation in PEG % the activation energy has increased consequently.

The below table has been formed with the obtained data for ionic conductivity and activation energy for pure LATP and varied percentages of PEG in LATP.

SI No.	PEG% (wt/wt)	Ionic conductivity at 30°C (S/cm)	Activation Energy (eV)
1	0	$5.486*10^{-5}$	0.44
2.	5	$9.399*10^{-6}$	0.34
3	10	$4.529*10^{-4}$	0.23
4	15	$1.347*10^{-5}$	0.50
5	25	$5.830*10^{-5}$	0.63

Here, in the table formulated above we can see that ionic conductivity for 5% PEG is lowest among all and the activation energy of PEG 10% is lowest among all with its ionic conductivity higher than PEG 5% we have further checked the charge discharge of PEG 10% (wt/wt) using symmetric cell with Li/LATP-10/Li configuration and electrochemical impedance spectroscopy before and after cycling.

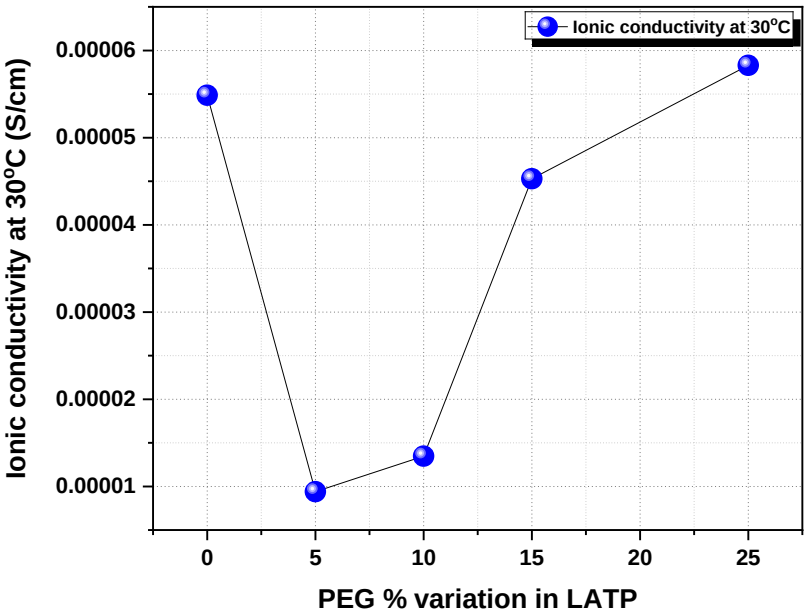


Figure 38: Ionic Conductivity VS PEG% variation plotted at room temperature(30°C)

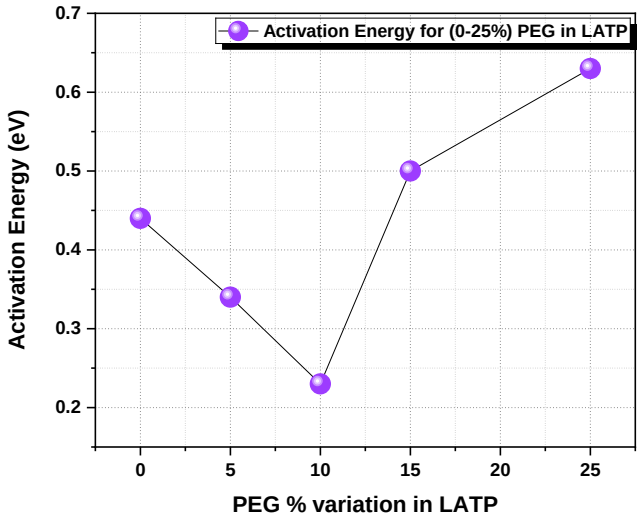


Figure 39: Activation Energy VS PEG% variation

4.4 Symmetric cell and stripping/plating of lithium

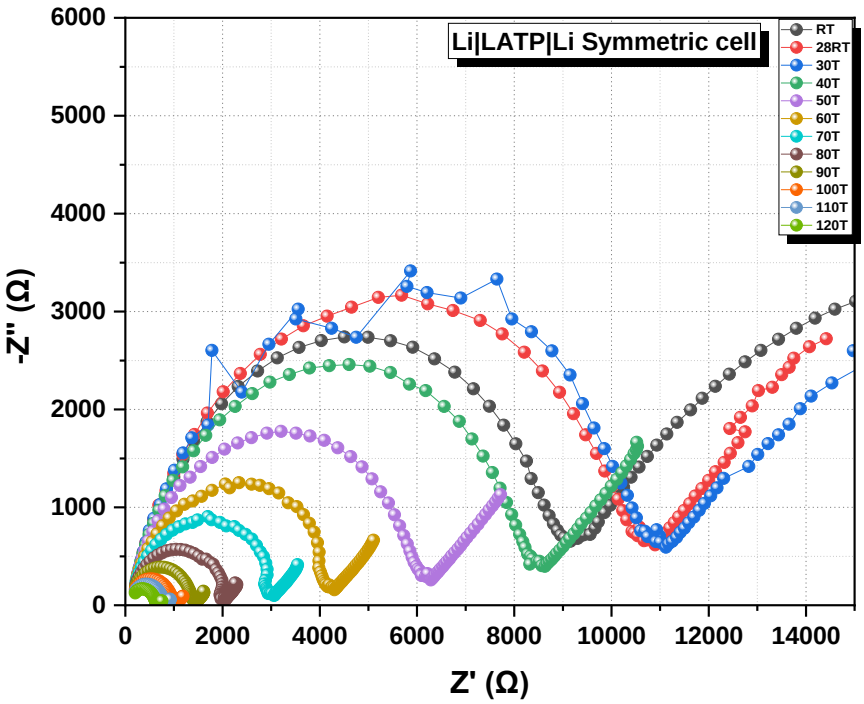


Figure 40: EIS for the symmetric cell of the pristine LATP cell (Li-LATP-Li)

The conductivity value for the symmetric cell of 19mm diameter pellet was fabricated inside an Argon facilitated 4-armed glove box. The conductivity value can be observed from RT to 120°C. A gradual decrease in the resistance can be observed with the drastic change from 6300 to 4200 at 60°C. So, the further symmetric cell is decided to run at 60°C.



Figure 41: Reaction between LATP and lithium foil in symmetric cell

When the symmetric cell of Li-LATP-Li was opened we can see a reaction has taken place on the solid-state electrolyte and Lithium foil resulting a black appearance on the white surface. This also indicate that the pure LATP electrolyte is not stable with the lithium foil. After sometime it was also observed that the EIS value has increased drastically when seen with temperature in comparison to the older EIS data.

4.5 Symmetric cell performance of Li/LATP-10/Li

To evaluate the electrochemical stability of LATP and various PEG percentages in LATP pellets with the Li anode during the Li plating/stripping process, Li||Li symmetric cells were assembled and cycled at 60°C under a current density of 198 µA/cm². The voltage profiles of Li||Li cells using 10 wt% PEG in LATP and pristine LATP pellets, shown in Figure, indicate a stable interface between Li and the LATP. Additionally, under the same current density, the polarization voltage of the Li||LATP-10||Li cell is lower than that of the cell with pure LATP electrolyte, suggesting lower resistance.

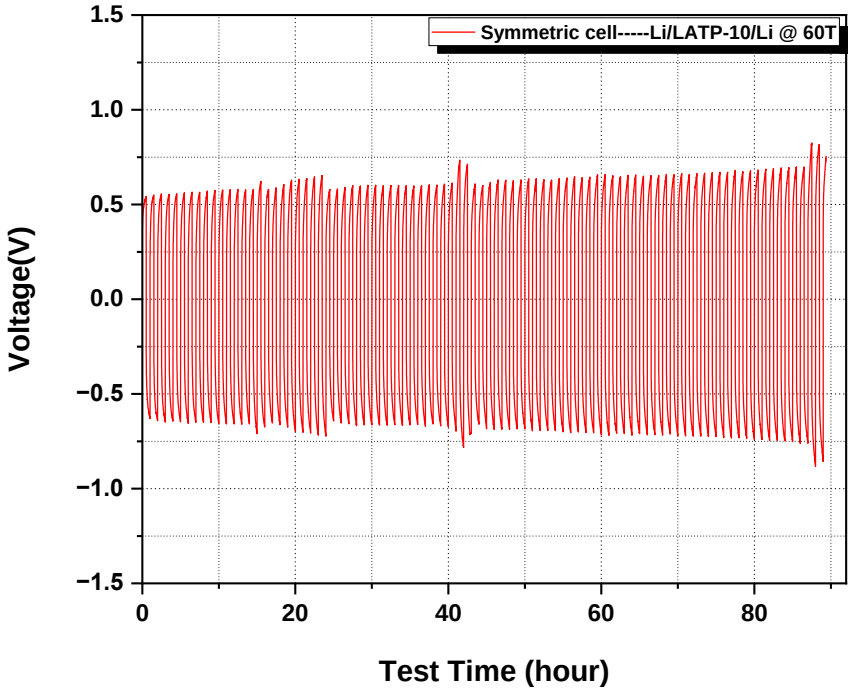


Figure 42: Electrochemical galvanostatic profile of Li/ LATP-10/Li symmetric cell

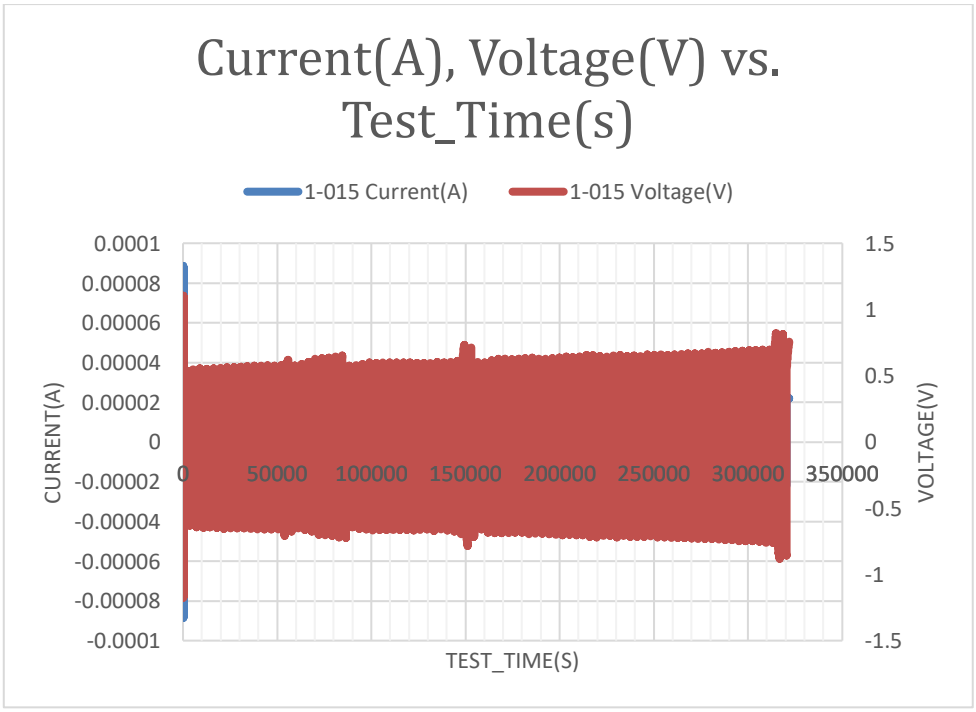


Figure 43: Current vs Time graph for the Li/LATP-10/Li for 90 hour

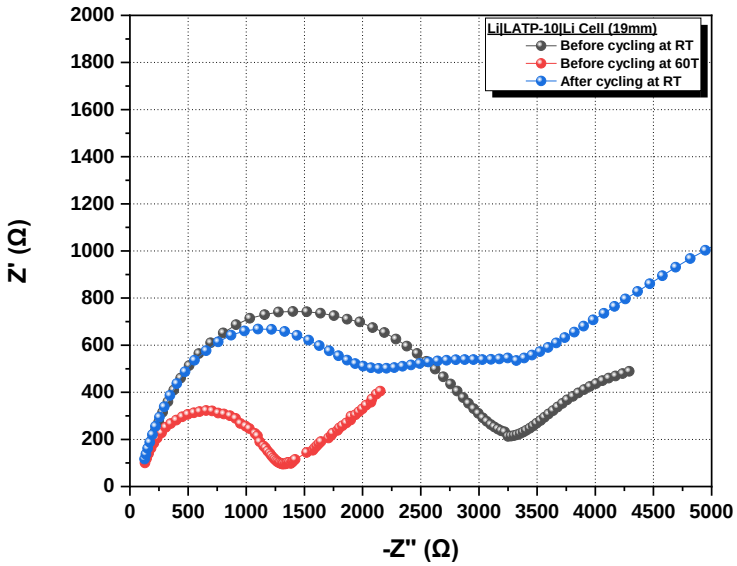


Figure 44: EIS for the symmetric cell of the LATP-10 cell (Li-LATP-10-Li)

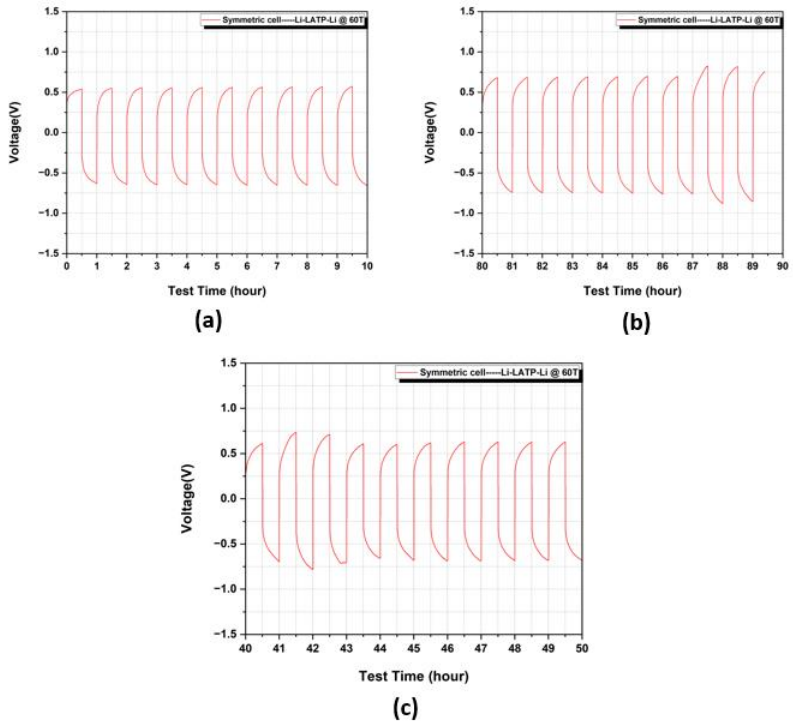


Figure 45: Enlarged cycling profiles from (a) 0-10hours [1st 10 hours]

(b)40-50 hours (c) 80-90hours [last 10 cycles]

The initial current density was set to 198 µA/cm² and maintained constant for 240 hours. The cycling was conducted with the following program: [charging at +198 µA/cm² for 30 minutes], rest (10 minutes), [discharging at -198 µA/cm² for 30 minutes], rest (10 minutes), within a voltage range of ±1.0 V. The positive and negative potentials in the curve indicate the Li stripping and plating processes, respectively.

In the Figure (a) the stripping /platting has been shown for the first 10hours followed by an intermediate cycle(figure b) and at last the end 10hours curve has been shown(Figure c).We can see that the polarization voltage of the solid-state electrolyte is 0.7V at a current density of 198 µA/cm² run for 90hours at both platting and stripping of lithium.

Symmetric cell performance of Li/LATP/Li

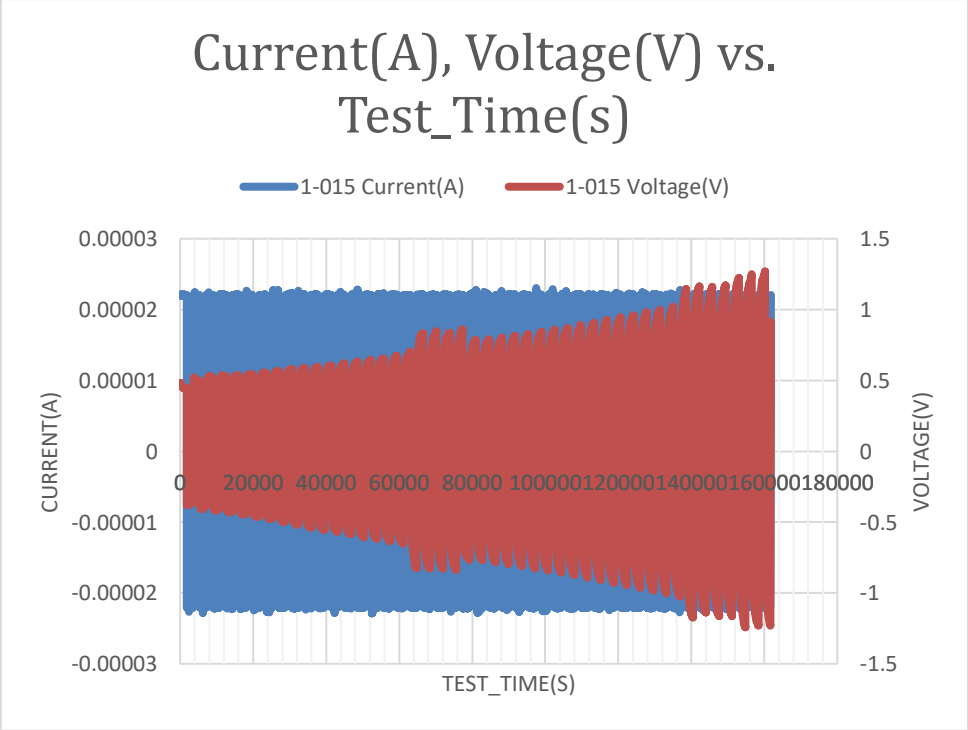


Figure 46: Current vs Time graph for the Li/LATP/Li for 45 hours.

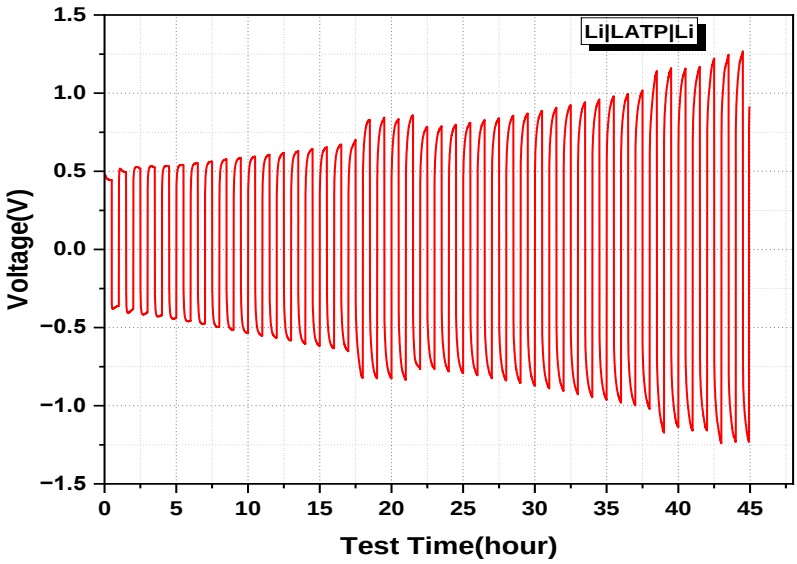


Figure 47: Electrochemical galvanostatic profile of Li/ LATP/Li symmetric cell

4.5 Post-electrochemical studies of the symmetric cell of pure LATP and varied concentration of PEG in LATP (Calendering effect)

We have performed a calendaring effect experiment on the symmetric cell of LATP and Lithium foil on both sides. We have prepared the 4 symmetric cells with the variation as i) pristine Li-LATP-Li (ii) Li-LATP+10PEG-Li (iii) Li-LATP+15PEG-Li & (iv) Li-LATP+25PEG-Li. The cell was kept in the room temperature for several days and at 5days interval the EIS of the cell was taken. The purpose of this experiment was to observe the growth of solid electrolyte interphase (SEI), the ageing of the crystallographic structure of the electrolyte material, impurities formation and dissolve in the electrolyte, unwanted chemical reaction between the Lithium foil and the electrolyte (this also predicts the interphase stability of the electrolyte with the lithium foil) and generation of other compounds if any.

We can already see that there is twice increase in the resistance value found in the EIS graph. This also predicts that unwanted reaction between the solid electrolyte and the Lithium foil has taken place making the symmetric cell highly unstable.

After day 15 we can see the resistance value has increased significantly for all the composition indicating highly unstable interphase of electrolyte and lithium foil. 3days later when we did another electrochemical impedance spectra the value did not come as a scattered plot was obtained making it clear that the electrolyte is no more in a stable condition for performance.

This main reason for this drastic change in ionic conductivity of the LATP when it is kept for several days exposed at atmospheric conditions the Ti $^{4+}$ get converted to Ti^{3+}.The titanium is coming from TiO_2 that was one of the precursor materials of LATP. This can also be checked using cyclic voltammetry by checking the oxidation and reduction peak of the graph.

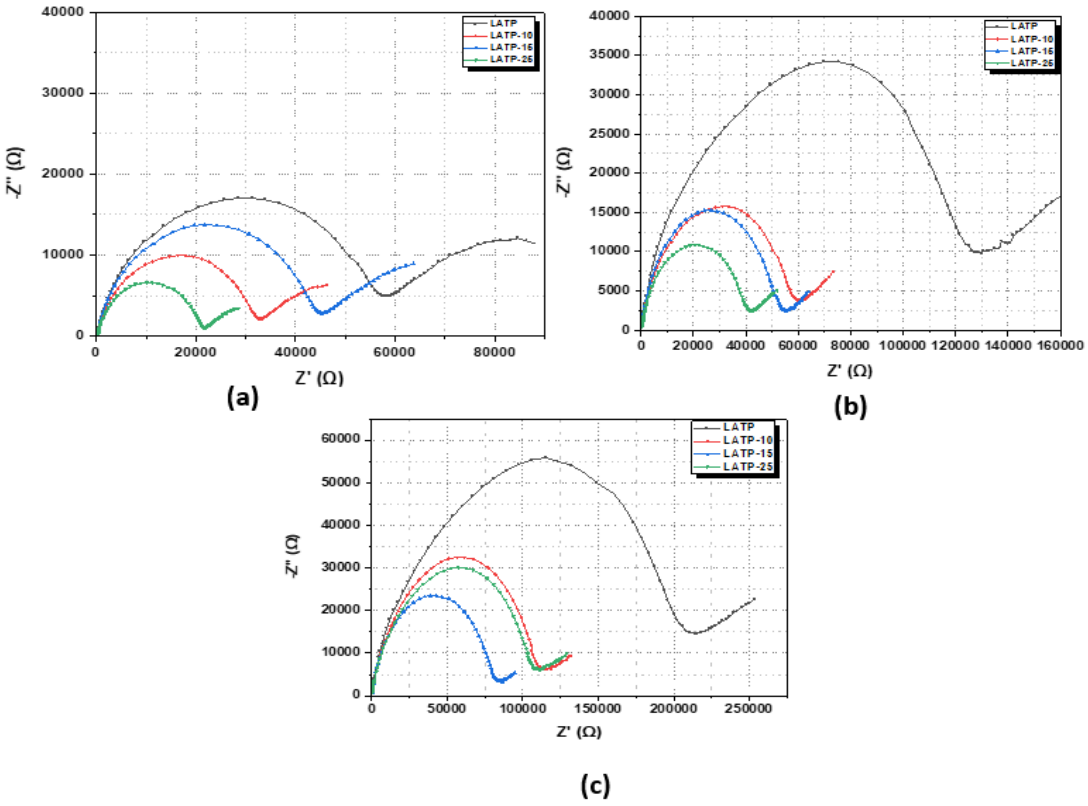


Figure 48: (a) DAY 1 (b)DAY 5 (c) DAY 10--EIS taken for the symmetric cell with pristine Li-LATP-Li & Li-LATP+PEG-Li

Conclusion

A brief study on NASICON type solid-state electrolyte named LATP with general formula as $Li_{1+x}Al_xTi_{2-x}(PO_4)_3$ was done. Initially the material was synthesized using all solid-state synthesis that is ball milling followed by calcination at higher temperature for 10hours. The formation of the single-phase material was confirmed from XRD data without any probable impurities like TiO_2 or $AlPO_4$ formation. Varied percentage of PEG-200 was added to pure LATP after 1st calcination at 500^oC and the morphology was studied. The particle size was analysed using DLS and the information regarding chemical bonds were observed from FTIR data. The density of the material was also checked using both green density method and Archimedes method. This confirmed the porosity of the material which have influence on the ionic conductivity of the material. The electrochemical studies of the solid-state electrolyte were done using symmetric cell and lithium metal on both side and LATP as solid-state electrolyte for all solid-state lithium-ion batteries (ASSLBs).

In the present research work the following are the inference or outcome as listed below:

- The most promising LATP solid-state electrolyte has been developed using glycine assisted advanced solid-state process.
  A single phase crystalline LATP powder obtained at 900^oC in air.
- The ionic conductivity of the developed LATP was found to be 10^{-4} S/cm at room temperature (30^oC). A decrease in activation energy could also be found in PEG-200 assisted synthesized LATP compared to LATP produced without LATP. The value of activation energy was measured to be 0.23eV for LATP-10 PEG compare to the value of LATP synthesized method (LATP: 0.44eV).
- The symmetric cell performance with the developed solid-state electrolyte LATP-10 delivered a stable charge discharge cycle over a constant current density of 198 µA/cm².
- LATP-10 produced low polarization voltage of 0.5V while cycling for 90hours.
- The overall study revealed that LATP produced using PEG assisted advance solid-state method resulted in engineered multifaceted

microstructure which might be responsible for facile Li^+ ion transport and lowering down of polarization voltage.

Therefore, it is evident that LATP synthesized by PEG-200 assisted solid-state process might be affected in making workable all solid-state batteries. (ASSBs)

Future works

The present study explored the possibility of making an engineered morphology of LATP solid-state electrolyte. The primary results as obtained was found to be encouraging and further extended to develop workable all solid-state lithium-ion metal batteries (ASSLMBs) by using LATP as solid inorganic electrolyte.

The future scope of further development of all solid-state batteries (ASSBs) lies in:

- Lithophilic functional layer in between lithium metal and inorganic solid-state LATP.
- A significant improvement is necessary in terms of sinterability and densification for developed LATP in all solid-state batteries (ASSBs).
- The scope of making LATP sintered body (less than 80 micron) probably be one of the options for its commercial success. Thus, a tape casting technique of making LATP sintered body might be employed on making a large surface area cell.

The author wish to pursue the above in her future research courses.

References

[1] Yang Jin, Kai Liu, Jialiang Lang, Xin Jiang, Zhikun Zheng, Qinghe Su, Zeya Huang, Yuanzheng Long, Chang-an Wang, Hui Wu and Yi Cui," High-Energy-Density Solid-Electrolyte-Based Liquid Li-S and Li-Se Batteries", Joule 4, 262–274

[2] Yu-Kun Liu, Chen-Zi Zhao, Juan Du, Xue-Qiang Zhang, Ai-Bing Chen,* and Qiang Zhang*," Research Progresses of Liquid Electrolytes in Lithium-Ion Batteries, Small 2023, 19, 2205315

[3] Xu K, **"Nonaqueous liquid electrolytes for lithium-based rechargeable batteries"***Chemical Reviews (2004) 104(10) 4303-4417*

[4] Fry, A. J. Synthetic Organic Electrochemistry, 2nd ed.; John Wiley: London, 1989

[5] J. Ming, Z. Cao, Y. Wu, W. Wahyudi, W. Wang, X. Guo, L. Cavallo, J. Y. Hwang, A. Shamim, L. J. Li, Y. K. Sun, H. N. Alshareef, ACS Energy Lett. 2019, 4, 2613.

[6] H. Zhao, X. Yu, J. Li, B. Li, H. Shao, L. Li, Y. Deng, J. Mater. Chem. A 2019, 7, 8700.

[7] M. Zhou, C. Qin, Z. Liu, L. Feng, X. Su, Y. Chen, L. Xia, Y. Xia, Z. Liu, Appl. Surf. Sci. 2017, 403, 260.

[8] S. Park, S. Y. Jeong, T. K. Lee, M. W. Park, H. Y. Lim, J. Sung, J. Cho, S. K. Kwak, S. Y. Hong, N. S. Choi, Nat. Commun. 2021, 12, 838.

[9] X. Li, X. P. Han, G. Li, J. Du, Y. Cao, H. C. Gong, H. L. Wang, Y. M. Zhang, S. Liu, B. S. Zhang, X. Y. Liu, P. Khangale, D. Hildebrandt, J. Sun, A. B. Chen, Small 2022, 18, e2202989.

[10] Zhang, N.; Beutl, A.; Rajinovic, K.; Kahr, J.; Jahn, M.; Nesoridi, M. Scalable Preparation of Practical 1Ah All-Solid-State Lithium-Ion Batteries Cells and Their Abuse Tests. J. Energy Storage 2023, 59, 106547.

[11]. Zhao, Y.; Huang, Z.; Chen, S.; Chen, B.; Yang, J.; Zhang, Q.; Ding, F.; Chen, Y.; Xu, X. A Promising PEO/LAGP Hybrid Electrolyte Prepared by a Simple Method for All-Solid-State Lithium Batteries. Solid State Ion. 2016, 295, 65–71.

[12] Jie, J.; Liu, Y.; Cong, L.; Zhang, B.; Lu, W.; Zhang, X.; Liu, J.; Xie, H.; Sun, L. High-Performance PVDF-HFP Based Gel Polymer Electrolyte with a Safe Solvent in Li Metal Polymer Battery. J. Energy Chem. 2020, 49, 80–88.

[13] Balakrishnan, N.T.M.; Das, A.; Joyner, J.D.; Jabeen Fatima, M.J.; Raphael, L.R.; Pullanchiyodan, A.; Raghavan, P. Quest for High-Performance Gel Polymer Electrolyte by Enhancing the Miscibility of the Bi-Polymer Blend for Lithium-Ion Batteries:Performance Evaluation in Extreme Temperatures. Mater. Today Chem. 2023, 29, 101407.

[14] Guo, M.; Dong, S.; Xiong, J.; Jin, X.; Wan, P.; Lu, S.; Zhang, Y.; Xu, J.; Fan, H. Flexible Core-Shell PAN/CNTs@PVDF-HFP/Uio 66-NH2 Hybrid Nanofibers Membrane for Advanced Lithium-Ion Batteries Separator. Mater. Today Chem. 2023, 30, 101552.

[15]. Wu, P.; Zhou, W.; Su, X.; Li, J.; Su, M.; Zhou, X.; Sheldon, B.W.; Lu, W. Recent Advances in Conduction Mechanisms, Synthesis Methods, and Improvement Strategies for Li1+xAlxTi 2−x (PO4)3 Solid Electrolyte for All-Solid-State Lithium Batteries. Adv. Energy Mater. 2023, 13, 2203440.

[16] Murata, K. An overview of the research and development of solid polymer electrolyte batteries. Electrochem. Acta 1995, 40, 2177–2184

[17] Ratner, M. A.; Johansson, P.; Shriver, D. F. Polymer electrolytes: Ionic transport mechanisms and relaxation coupling. MRS Bull. 2000, 25, 31–37.

[18] Quartarone, E.; Mustarelli, P. Electrolytes for solid-state lithium rechargeable batteries: Recent advances and perspectives. Chem. Soc. Rev. 2011, 40, 2525–2540.

[19] Ehrenstein, G. W.; Theriault, R. P. Polymeric materials: Structure, Properties, Applications; Hanser Carl GmbH + Co: Erlangen, 2001; pp 67–78.

[20] a) Z. Xue, D. He, X. Xie, J. Mater. J. Mater. Chem. A 2015, 3, 19218; b) E. Quartarone, P. Mustarelli, Chem. Soc. Rev. 2011, 40, 2525.

[21] L. Long, S. Wang, M. Xiao, Y. Meng, J. Mater. Chem. A 2016, 4, 10038.

[22] N. Imanishi, S. Hasegawa, T. Zhang, A. Hirano, Y. Takeda, O. Yamamoto, Lithium anode for lithium-air secondary batteries, J. Power Sources, 185 (2008) 1392-1397.

[23] Y. Zhu, X. He, Y. Mo, Origin of outstanding stability in the lithium solid electrolyte materials: insights from thermodynamic analyses based on first-principles calculations, ACS Appl. Mater. Interfaces, 7 (2015) 23685-23693

[24] Jurgen Peter Gross, Jurgen Malzbender, Enkhtsetseg Dashjav, Frank Tietz and Ruth Schwaiger, Conductivity, microstructure and mechanical properties of tape-cast LATP with LiF and SiO2 additives, J Mater Sci (2022) 57:925–938

[25] Andr´es Mormeneo-Segarra, Sergio Ferrer-Nicomedes, Sonia Simon, Nuria VicenteAgut, Juan Carlos Jarque-Fonfría, Antonio Barba-Juan, Using in operando impedance spectroscopy technique to unravel the sintering process evolution of Bi2O3: LATP cold-sintered solid electrolyte, Solid State Ionics 406 (2024) 116482

[26] Yulong Liu, Jingru Liu, Qian Sun, Dawei Wang, Keegan R. Adair, Jianneng Liang, Cheng Zhang, Li Zhang, Shigang Lu, Huan Huang, Xiping Song, and Xueliang Sun, Insight into the Microstructure and Ionic Conductivity of Cold Sintered NASICON Solid Electrolyte for Solid-State Batteries, *ACS Appl. Mater. Interfaces* 2019, 11, 31, 27890–27896

[27] Yasmine Benabed, Maxime Rioux, Steeve Rousselot, Geoffroy Hautier and Mickaël Dollé, Assessing the Electrochemical Stability Window of NASICON-Type Solid Electrolytes Frontiers in Energy Research May 2021 | Volume 9 | Article 682008